General Disclaimer

One or more of the Following Statements may affect this Document

- This document has been reproduced from the best copy furnished by the organizational source. It is being released in the interest of making available as much information as possible.

- This document may contain data, which exceeds the sheet parameters. It was furnished in this condition by the organizational source and is the best copy available.

- This document may contain tone-on-tone or color graphs, charts and/or pictures, which have been reproduced in black and white.

- This document is paginated as submitted by the original source.

- Portions of this document are not fully legible due to the historical nature of some of the material. However, it is the best reproduction available from the original submission.

NASA CR-114288

AVAILABLE TO THE PUBLIC

INVESTIGATION OF LINE-OF-SIGHT PROPAGATION IN DENSE ATMOSPHERE: PHASE II

FINAL REPORT

BY

J. W. DAVENPORT AND D. A. DE WOLF

JULY 1971

PREPARED UNDER CONTRACT NO. NAS 2-5310

RCA LABORATORIES
PRINCETON, NEW JERSEY 08540

AMES RESEARCH CENTER
MOFFETT FIELD, CALIFORNIA
NATIONAL AERONAUTICS AND SPACE ADMINISTRATION

1. Report No.	2. Government Accession No.	3. Recipient's Catalog No.
Phase II Final Report		

4. Title and Subtitle	5. Report Date
Investigation of Line-Of-Sight Propagation In Dense Atmosphere: Phase II	July 1971
	6. Performing Organization Code
7. Author(s)	8. Performing Organization Report No.
J. W. Davenport and D. A. DeWolf	
9. Performing Organization Name and Address	10. Work Unit No.
RCA Laboratories Princeton, New Jersey 08540	11. Contract or Grant No. NAS 2-5310
	13. Type of Report and Period Covered
12. Sponsoring Agency Name and Address	Final Report June 1970 - Feb. 1971
Ames Research Center Moffett Field, California	14. Sponsoring Agency Code NASA CR-114288

15. Supplementary Notes

16. Abstract

The investigation of the effect of Jupiter's atmosphere upon communications in the 1 to 10 GHz frequency band initiated previously was continued in Phase II of the study. Microwave absorption and decimetric-radio noise have been singled out for special attention. Laboratory measurements of the absorption in simulated Jovian atmospheres have been carried out at S-band. These were integrated with recent X-band data to yield a complete picture of the absorption given a model atmosphere. The previously reported results for Venus have been updated. Conclusions of the investigation are: (1) Absorption losses in Jupiter's supra-cloud atmosphere at S- and X-band frequencies are very important; 1 dB to 10 dB for vertical propagation terminating at the cloud layer. These losses are due to nearly-saturated ammonia at the prevelant pressures and they increase rapidly as the altitude decreases toward the cloud layer. These losses would increase still further if the temperatures are higher than the hypothesized 170°K at the cloud layer. These conclusions have been substantiated by laboratory measurements in a simulated Jovian environment. (2) Jovian decimetric noise in the region of 2 GHz and higher frequencies can be ignored by spaceprobes with isotropic antennas. Unless the receiver front end is strongly cooled, internal-set noise prevails. However, directional antennas on probes beyond Jupiter can suffer from Jovian-noise interference prior to occultation by the planet. The effect in this case is strongly dependent upon antenna-dish size. The noise sources are relativistically accelerated electrons spiralling around Jovian magnetic field lines and emitting synchrotron radiation. (3) Turbulence-induced signal fading in the Venusian atmosphere exceeds 15 dB at 2 GHz and higher frequencies when signal paths traverse the 15 to 20 km altitude region, despite uncertainties in frequency scaling and the amount of turbulence below 15 km altitude. Phase 2 Jupiter propagation-loss determinations are confined to the upper-atmosphere models of Moroz. Loss factors corresponding to the deeper atmosphere (JPL/Lewis) models will be reported under Phase 3. The Venera-5 and -6 measurements predict less fading, as do the Mariner-5 measurements (but the latter measurements have smoothed out most of the effects of turbulence); however, the estimates are based on the actually measured "worst-case" Venera-4 data.

17. Key Words (Selected by Author(s))	18. Distribution Statement
dense planetary atmosphere propagation ammonia absorption	

19. Security Classif. (of this report)	20. Security Classif. (of this page)	21. No. of Pages	22. Price*
Unclassified	Unclassified	62	

ACKNOWLEDGMENT

The authors wish to express their sincere thanks to Dr. A. A. Maryott of the National Bureau of Standards, Gaithersberg, Md., for making available both equipment and data. In addition, he offered numerous helpful comments on the absorption problem generally.

Investigation of Line-of-Sight Propagation
in Dense Atmosphere: Phase II

by

J. W. Davenport and D. A. deWolf
RCA Laboratories
Princeton, New Jersey

SUMMARY AND CONCLUSIONS

The investigation of the effect of Jupiter's atmosphere upon communications in the 1 to 10 GHz frequency band initiated previously was continued in Phase II of the study. Microwave absorption and decimetric-radio noise have been singled out for special attention. Laboratory measurements of the absorption in simulated Jovian atmospheres have been carried out at S-band. These were integrated with recent X-band data to yield a complete picture of the absorption given a model atmosphere. The previously reported results for Venus have been updated.

Conclusions of the investigation are:

(1) Absorption losses in Jupiter's supra-cloud atmosphere at S- and X-band frequencies are very important; 1 dB to 10 dB for vertical propagation terminating at the cloud layer. These losses are due to nearly-saturated ammonia at the prevelant pressures and they increase rapidly as the altitude decreases toward the cloud layer. These losses would increase still further if the temperatures are higher than the hypothesized 170°K at the cloud layer. These conclusions have been substantiated by laboratory measurements in a simulated Jovian environment.

(2) Jovian decimetric noise in the region of 2 GH_z and higher frequencies can be ignored by spaceprobes with isotropic antennas. Unless the receiver front end is strongly cooled, internal-set noise prevails. However, directional antennas on probes beyond Jupiter can suffer from Jovian-noise interference prior to occultation by the planet. The effect in this case is strongly dependent upon antenna-dish size. The noise sources are relativistically accelerated electrons spiralling around Jovian magnetic field lines and emitting synchrotron radiation.

(3) Turbulence-induced signal fading in the Venusian atmosphere exceeds 15 dB at 2 GHz and higher frequencies when signal paths traverse the 15 to 20 km altitude region, despite uncertainties in frequency scaling and the amount of turbulence below 15 km altitude.

Phase 2 Jupiter propagation-loss determinations are confined to the upper-atmosphere models of Moroz. Loss factors corresponding to the deeper atmosphere (JPL/Lewis) models will be reported under Phase 3.

TABLE OF CONTENTS

TABLE OF CONTENTS (Continued)

LIST OF ILLUSTRATIONS

LIST OF ILLUSTRATIONS (Continued)

GLOSSARY OF TERMS AND SYMBOLS

a	broadening coefficient	$MH_z(Torr)^{-1}$
c_p	specific heat at constant pressure	$J\ kg^{-1}{}^oK^{-1}$
c_v	specific heat at constant volume	$J\ kg^{-1}{}^oK^{-1}$
f	frequency	Hz
h	scale height	km
n	refractive index	(dimensionless)
B	magnetic field	Gauss = 10^{-4}Weber m^{-2}
J		Joule
N	molecular density	m^{-3}
N	refractivity	(dimensionless)
N		Newton
P	power	W
P	pressure	Nm^{-2}
S	flux	Wm^{-2}
W		watt
α	absorption coefficient	cm^{-1} or $dB\ km^{-1}$
γ	collision frequency	Hz
γ	c_p/c_v	(dimensionless)
γ	$(1 - v^2/c^2)^{-1/2}$	(dimensionless)
γ_a	adiabatic temperature gradient	$^oK\ km^{-1}$
μ	dipole moment	coulomb-m
ν	frequency	Hz
σ_ε	signal power standard deviation	dimensionless
ζ	frequency	Hz
z	height	km

I. MICROWAVE ABSORPTION

A. INTRODUCTION

From the point of view of communications, microwave absorption by gases along the path between transmitter and receiver is very important. It is one of the fundamental limitations on a system, and its behavior with frequency is an important design parameter. In the presence of an absorber which is not too strong, the power in an electromagnetic wave will decay exponentially along the path.

$$P(L) = P(0) \exp\left[-\int_0^L dx\, \alpha\,(x)\right] \tag{1}$$

The total signal loss along a path is then given by

$$A(\text{in dB}) = -10 \log\,[P(L)/P(0)] = 4.34 \int_0^L dx\, \alpha\,(x) \tag{2}$$

α is often given in cm^{-1}, however according to Eq. (2) 1 cm^{-1} corresponds to 4.34×10^5 dB/km. For example, in the earth's atmosphere the absorption due to water vapor at 10 GHz typically amounts to about 0.0025 dB/km. At S-band it is much lower, about 0.0004 dB/km. As shown below, in the Jovian atmosphere at cloud level, the absorption at S-band is about 0.05 dB/km and at X-band about 0.6 dB/km.

The coefficient α can be approximately written as

$$\alpha(\vec{r},\nu) \overset{\sim}{=} N(\vec{r}) f(\nu)$$

$\vec{r}$ = position

ν = frequency

where $N(\vec{r})$ is the number density of absorbing molecules and $f(\nu)$ is a function characteristic of the chemical species of the molecule. Clearly $N(\vec{r})$ involves the composition of the atmosphere and the distribution of the various species. On the other hand, $f(\nu)$ is a parameter obtained from laboratory absorption measurements.

There has been interest in this problem for some time (ref. 1) because it relates to the determination of the brightness temperature of

the planet. Unfortunately, these calculations are not directly applicable to the absorption problem encountered in communications. For one thing, the brightness-temperature calculations are restricted to frequencies above 10 GHz because non-thermal sources near the planet produce most of the flux at lower frequencies. Yet the theory of the absorption coefficient may not be as good at the lower frequencies, because laboratory data are lacking. In addition, the brightness temperature of an optically thick layer of gas (which is the case for Jupiter's atmosphere) is not as sensitive to the absorption coefficient as the signal loss in propagating through the layer. The brightness temperature of a layer can be written

$$T_b = T_o \left[1 - \exp\left(-\alpha L\right)\right] \tag{3}$$

Here T_o is the actual gas temperature, T_b the brightness temperature, α the absorption coefficient, and L the layer thickness. The product αL is called the optical depth which is about 7 for Jupiter above the clouds (ref. 2). Notice that in the limit of infinite L, the brightness temperature is *independent* of α, and equal to the gas temperature. However, a signal passing through the layer would decay according to Eq. (1) and the received power is quite *sensitive* to α. So, the absorption calculations cannot be simply taken over from the brightness temperature calculations - they must be extended. In this report, the absorptive signal loss which a space craft would experience will be calculated for several frequencies and several geometries all of which reflect actual plans for Pioneer F and G. First, various model atmospheres are considered and a model chosen for actual calculations. However, results are presented in a form which makes them relatively independent of the particular model used. Then, a detailed calculation of the ammonia absorption coefficient will be presented. Finally, possible uncertainties in the calculations are mentioned including an uncertainty in the superrefractive height.

B. MODEL ATMOSPHERES

An excellent analysis of the state of the various model atmospheres has been given by Goodman (ref. 3). Other sources on models are Michaux, Moroz, and Trafton (refs. 4,5,6). A recent discussion of the constituents of the atmosphere has been given by Owen (ref. 7).

For our purposes the following is an adequate description of the atmosphere. Jupiter is surrounded by a cloud layer thought to be several thousand km above the surface (ref. 8). Above the clouds is a relatively clear atmosphere consisting almost entirely of hydrogen and helium.

The temperature at the upper surface of the clouds is approximately 170°K and the pressure there is of the order of 2 atm (1 atm ≡ 760 Torr ≡ 760 mm-Hg). The constituents and their amounts* are $[H_2] = 85 \pm 15$ km-atm, [He] = 10 to 100 km-atm, $[CH_4] = 0.050$ km-atm and $[NH_3] \simeq 0.007$ km-atm. These are values given by Owen (ref. 7); notice the uncertainty in the helium concentration, it is taken into account in all our calculations. Clearly, the atmospheric processes are dominated by H_2 and He. However the absorption both at microwave and infrared frequencies is controlled by the NH_3 and CH_4.

In the stratosphere (T = constant) the pressure and density follow an exponential law

$$P(z) = P(0) \exp(-z/h) \tag{4}$$

where $h = \frac{kT}{mg} \equiv$ scale height.

Here $k = 1.38 \times 10^{-23}$ Joules $(°K)^{-1}$, m is the molecular mass, and $g = 26 m (sec)^{-2}$. For H_2, $h \simeq 28$ km. For NH_3, h is much less because m is greater. However, the ammonia distribution is not governed by Eq. (4) because of the saturation effects discussed below. Jupiter probably has an atmosphere above the cloud layer in which the temperature varies linearly with height

$$T(z) = T(0) - \gamma_a z$$

$$\gamma_a = g/c_p \equiv \text{adiabatic temperature gradient} \tag{5}$$

$$c_p = \text{specific heat at constant pressure}$$

This troposphere would be expected to be about 20 to 30 km thick. Since c_p is about 10^4 Joules $(kg\ °K)^{-1}$, γ_a is about 2.5 $°K(km)^{-1}$. In the troposphere, the pressure is related to the temperature by the adiabatic law

$$P = P(0) [T/T(0)]^{\gamma/(\gamma-1)} \tag{6}$$

* 1 km-atm ≡ $2.69 \times 10^{28} m^{-2}$. It is a measure of the number of molecules in the atmosphere per unit surface area of the planet. For convenience this is converted into the length of the column which would be obtained if the gas were compressed to STP. For 1 km-atm this length is 1 km.

where γ is the ratio of specific heats at constant pressure and volume ($\gamma = 1.4$ for H_2).

There is evidence (ref. 7) that the ammonia vapor is saturated near the cloud tops. This means that its partial pressure is just the vapor pressure which can be obtained from the Clausius-Clapeyron equation. Specializing to the solid-gas transition

$$P(NH_3) = P_o \exp [-23(T_o/T-1)] \tag{7}$$

The subscript o refers to cloud top-values. P_o is about 2.4 Torr if T_o is taken to be 170°K (ref. 15). The number of molecules per unit volume, N, is given by $N = P(kT)^{-1}$.

Goodman (ref. 3) has discussed the various possible absorbers at microwave frequencies and shown that ammonia is by far the strongest. To be sure, water vapor absorbs at these frequencies but even if there were equal amounts of water and ammonia the absorption due to H_2O would be only about 2% of that due to NH_3. Hydrogen also has a collision-induced absorption spectrum but it is not important below about 10 GHz.

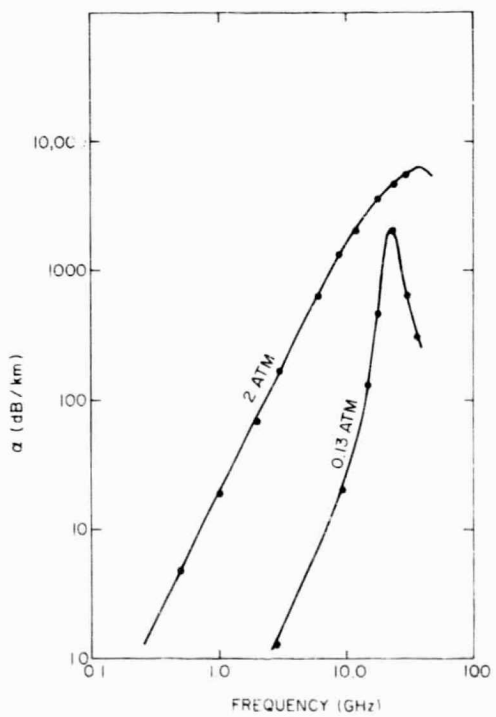

Figure 1. Absorption coefficient, α versus frequency for pure ammonia at two different pressures (from ref. 11).

C. THE AMMONIA ABSORPTION COEFFICIENT

The absorption spectrum of ammonia at microwave frequencies arises from a molecular transition called inversion. The molecule has a "pyramid" shape with the three hydrogens forming a basal plane. The nitrogen may then oscillate between positions above and below the basal plane. This is the inversion transition which results in some 66 spectral lines between 17 and 40 GHz. The absorption at any frequency is the sum of the contributions from the individual lines. Ordinarily, the absorption is important only for frequencies near resonance. However, the spectral lines may be considerably broadened by collisions, which become more important at high pressure. For example, the oxygen line near 60 GHz is pressure-broadened in the earth's atmosphere and contributes to the absorption throughout the microwave region. The absorption coefficient for pure ammonia at two different pressures is shown in Fig. 1, clearly demonstrating the broadening effect.

The theory of the absorption coefficient has been outlined by Townes and Schawlow (Ref. 9). The result for a single line near resonance is

$$\alpha_{ij} = \frac{\pi f_i |\mu_{ij}|^2}{3c\ kT\ \varepsilon_o} N\nu^2 \frac{\gamma_{ij}}{(\nu-\nu_{ij})^2 + \gamma_{ij}^2} \qquad (8)$$

μ_{ij} = dipole moment matrix element (coulomb-m)
f_i = fraction of molecules in the lower state
$c = 3 \times 10^8$ m/sec
$\varepsilon_o = 8.85 \times 10^{-12}$ farad m^{-1}
N = absorbing molecules per unit volume (m^{-3})
ν = frequency (Hz)
ν_{ij} = resonance frequency
γ_{ij} = collision frequency (Hz) = $(2\pi\tau)^{-1}$
τ = collision lifetime (sec)

This function is sharply peaked at $\nu = \nu_{ij}$ and the half width at half maximum is γ_{ij}. The total absorption coefficient is obtained by summing over all transitions $i \rightarrow j$, with resonance frequencies ν_{ij}. The collision frequency is the product of molecular density, thermal velocity, and collision cross section i.e., $\gamma_{ij} = N_s v\ \sigma_{ij}$. N_s is the number of scattering molecules per unit volume (which may be different from N, the number of absorbing molecules). Actually, expression (8) must be modified in order to give an accurate representation of the absorption. This will be carried out in Section II. But (8) reproduces the important features i.e., those relevant to communications. First, α is directly

proportional to $N = p(kT)^{-1}$ where p is the partial pressure of the absorber. For example, near the cloud layer the ammonia partial pressure rises exponentially with height according to Eq. (7). Therefore a large increase in absorption is expected there. Second, for frequencies below resonance, the absorption increases approximately as ν^2. Therefore the absorption in dB/km increases by a factor of roughly 20 from S-band to X-band. Finally, provided the pressure is below about 10 atm, the absorption increases linearly with γ_{ij} which in turn is proportional to the partial pressure of the scattering gas. To take account of a mixture of gases we write

$$\gamma = \gamma_{NH_3} + \gamma_{H_2} + \gamma_{He}$$
$$\gamma = a_{NH_3} P_{NH_3} + a_{H_2} P_{H_2} + a_{He} P_{He} \qquad (9)$$

where the pressures are partial pressures, and the coefficients a are temperature dependent. It is the increase in γ with pressure which leads to the term "pressure broadening". It was remarked previously that 66 lines have been found in the NH_3 inversion spectrum. Therefore the sum $\alpha = \Sigma\alpha_{ij}$ is tedious to calculate. One simplification that can be made is to replace the ν_{ij} and γ_{ij} by average values, γ and ν_o. Then the sum becomes

$$\alpha = \frac{\pi}{3c\ kT\ \varepsilon_o} N\nu^2 \left[\sum f_i |\mu_{ij}|^2\right] \frac{\gamma}{(\nu-\nu_o)^2 + \gamma^2} \qquad (10)$$

The sum in brackets has been performed (ref. 33) for the most intense lines; the result is

$$\sum f_i |\mu_{ij}|^2 \cong 0.40\ \mu^2$$

where $\mu = 4.90 \times 10^{-30}$ coulomb-m is the dipole moment of the non-vibrating molecule.

In order to obtain a ($\gamma = aP$) experiments were carried out in which α was actually measured by a cavity technique. The details are contained in Section II and the results are shown in Fig. 2 where α is plotted as a function of frequency for the region near the cloud layer. The ammonia partial pressure was taken to be 2 Torr and the temperature 170°K. The partial pressures of H_2 and He were assumed to be 2.0 atm and 1.44 atm respectively. All of these correspond to the model of Moroz (ref. 5). For comparison the water-vapor absorption coefficient for *earth* on a typical day is included (refs. 9, 16).

A similar procedure has been used by Wrixon (ref. 13) to calculate Jupiter's radio brightness temperature.

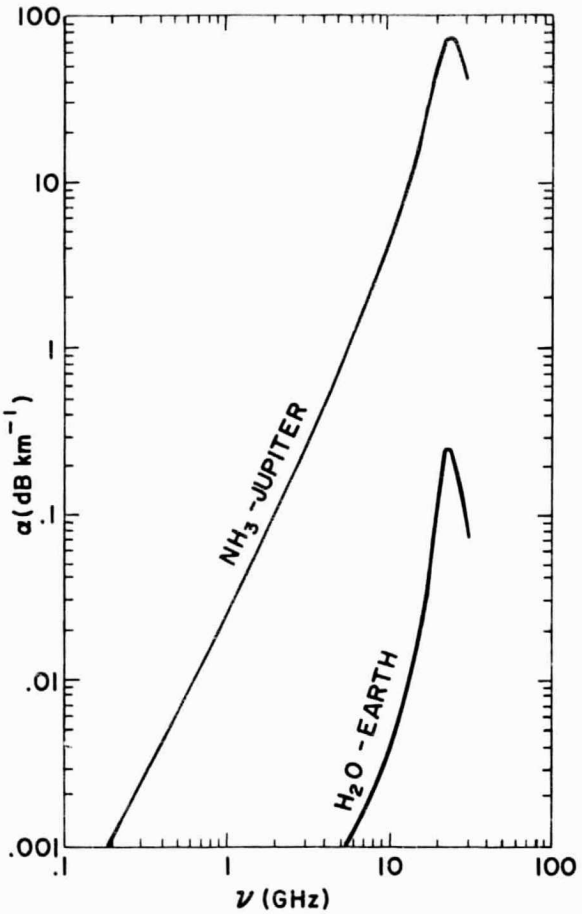

Figure 2. Absorption coefficient α versus frequency at the Jovian cloud top. P_{H_2} = 2 atm, P_{He} = 1.4 atm, P_{NH_3} = 2 Torr, T = 170°K. For comparison, the absorption due to a mixture of water vapor in air for a typical earth day is shown. The water vapor partial pressure is about 9 Torr.

D. RESULTS

We now have all the information required for the calculation of the total absorption in each case. The absorption coefficient at the cloud tops is shown in Fig. 2. The variation with height is assumed to be due completely to N and is given by Eq. (7). This should be a valid approximation because the NH_3 concentration changes drastically with height compared to the broadening parameters which vary with

the hydrogen concentration. The change in N with height is given through Eqs. (5) and (7) by

$$N(z) = N(0) \frac{T_o}{T_o - \gamma_a z} \exp \left[-23 \left(\frac{T_o}{T_o - \gamma_a z} - 1 \right) \right] \qquad (12)$$

The absorption is given by Eq. (2). In evaluating the integral in Eq. (2), two different geometries are assumed - occultation and direct or vertical. The result can be written

$$A(\text{in dB}) = \alpha(\nu, z)\, L_{eff}$$

where $\alpha(\nu,z)$ is the absorption coefficient at the lowest point on the ray path, (dB km^{-1}) and L_{eff} is the effective path length. Carrying out the integral it is found that

$$L_{eff} \cong \begin{cases} T_o/23\gamma_a \sim 3 \text{ km "direct"} \\ [2\pi R\, T_o/23\gamma_a]^{1/2} \sim 1100 \text{ km "occultation"} \end{cases}$$

where $R \cong 71{,}300$ km is the planetary radius.

These results are shown in Figs. 3 and 4 where z is the distance of closest approach of the ray from the cloud top. For the vertical geometry, z is simply the distance of the transmitter from the cloud top. Notice that in Eq. (12) z may become negative, which then measures distances below the cloud level. The results have been plotted as a function of temperature because there is some uncertainty as to the temperature of the cloud layer. Corresponding values of height according to the model of Moroz (ref. 5) are given in the figure. If the Moroz model is followed completely, the cloud-top temperature is 170°K and the absorption for an occultation experiment is 160 dB at S-band. However, other authors find lower temperatures, e.g., Trafton finds 158°K which implies ≈30 dB attenuation. The unfortunate result is that slight uncertainties in temperature produce large uncertainties in signal loss. Apparently better model atmospheres will be needed before this uncertainty can be reduced.

E. LOWEST POINT

In an occultation experiment it is of interest to know what the lowest point probed will be. This depends on the power available on

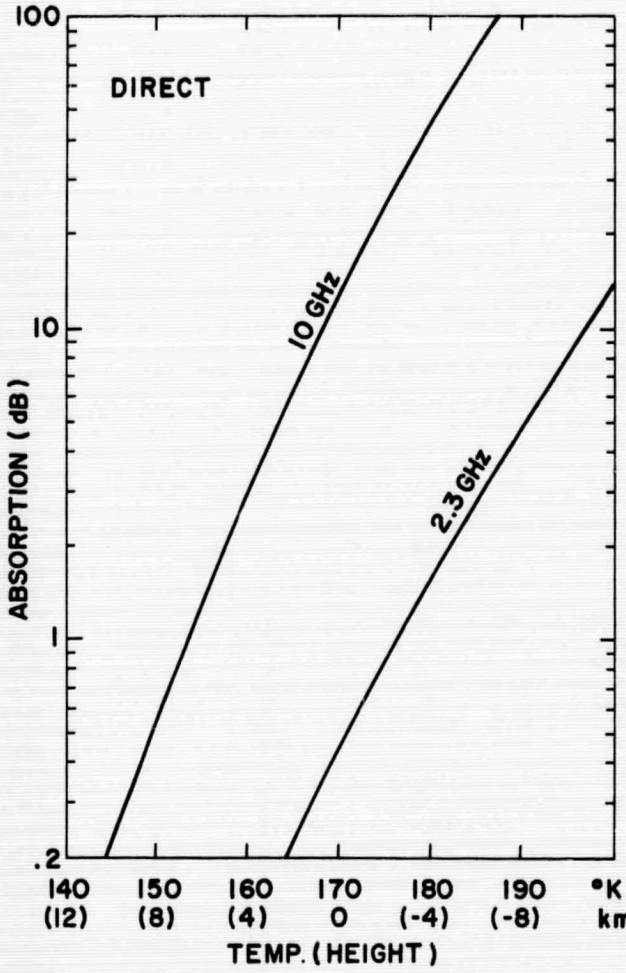

Figure 3.

Total absorption for direct paths through the atmosphere versus temperature at the probe. In parentheses are the heights above and below the cloud layer which correspond to each temperature according to the model of Moroz.

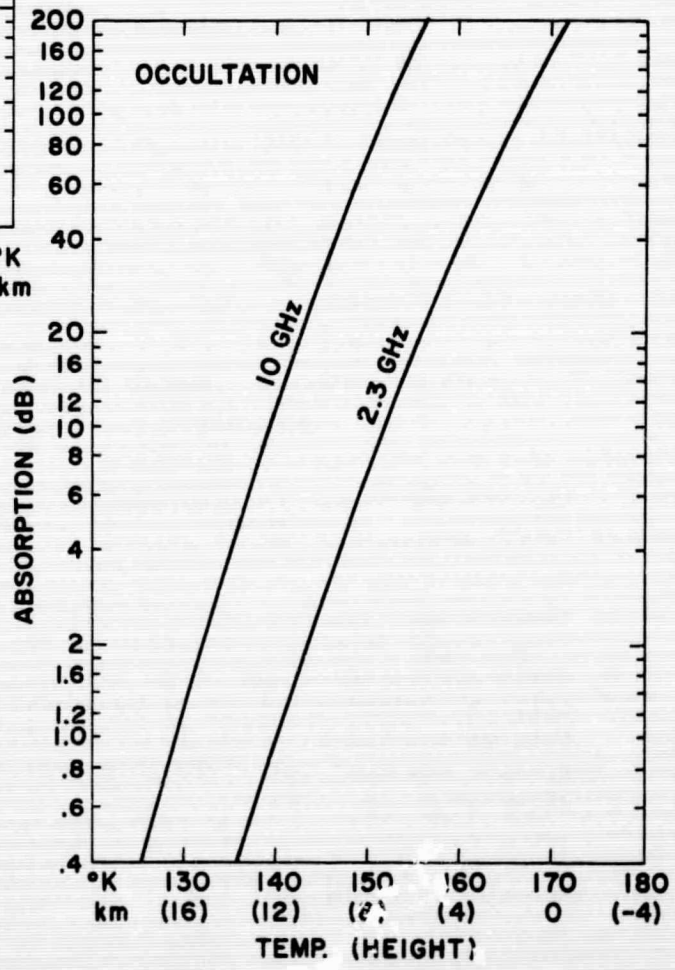

Figure 4.

Total absorption for occultation paths versus temperature at the lowest height probed. In parentheses are the heights above and below the cloud layer which correspond to each temperature according to the model of Moroz.

the spacecraft and the refractive properties of the atmosphere. For example, the atmosphere may be super-refractive (as with Venus). This means that rays parallel to the surface and lower than the super-refractive height are bent into the surface of the planet. If such an effect exists on Jupiter, it will be hard to describe accurately because the super-refractive height depends critically on the amount of helium -- a quantity which is not well known. Figure 5 shows the super-refractive height as a function of the ratio of He to H_2, assuming an exponential

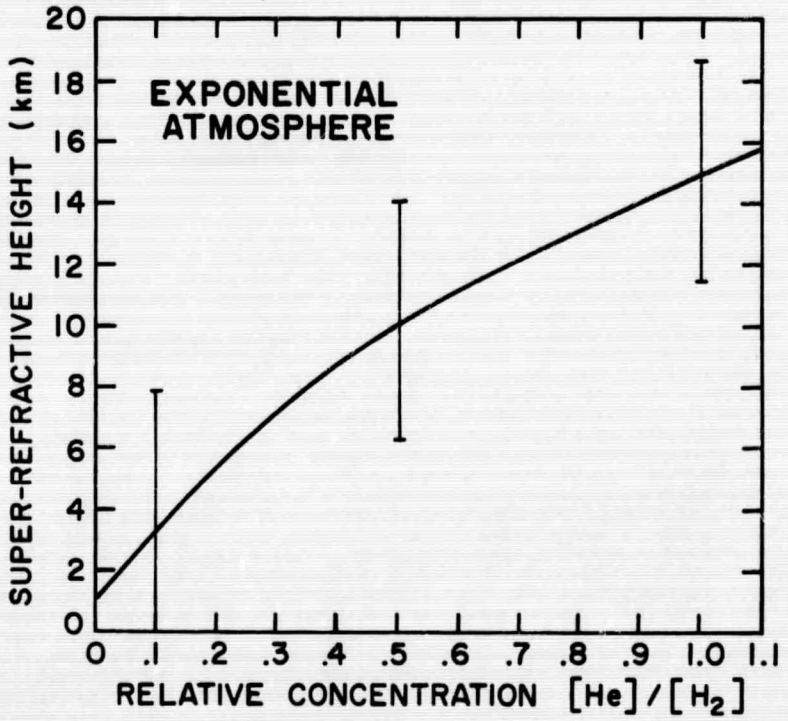

Figure 5. Super-refractive height versus relative concentration of He. For the Moroz model $[He]/[H_2] = 0.36$.

atmosphere. The figure shows that the actual value of the super-refractive height depends critically on the model chosen. The conclusion is qualitatively the same if an adiabatic model atmosphere is used. The critical height is obtained by equating the curvature of the ray with that of the planet. For lower altitudes the ray curvature will be greater and must therefore intersect the planet. The ray curvature is given by

$$K_r = \frac{1}{n} \left|\frac{\partial n}{\partial z}\right| = \frac{1}{R} \qquad (13)$$

where R is the planetary radius and n is the refractive index. For an exponential atmosphere

$$n = 1 + N_o e^{-z/h} \quad \text{and} \quad N_o \ll 1 \tag{14}$$

then

$$\frac{1}{R} \approx \frac{N_o e^{-z_c/h}}{h} \tag{15}$$

which fixes z_c - the critical height. Similarly, for an adiabatic atmosphere

$$n = 1 + N_o \left[\frac{T_o - \gamma_a z}{T_o}\right]^{1/(\gamma-1)} \tag{16}$$

then

$$\frac{1}{R} \approx \frac{N_o \gamma_a}{T_o(\gamma-1)} \left[1 - \gamma_a z_c / T_o\right]^{(2-\gamma)/(\gamma-1)} \tag{17}$$

which again fixes z_c. However, as indicated previously, z_c can only be said to be within 10 to 15 km of the cloud layer depending on the model assumed. The exact height will have to await a better determination of the helium concentration. If that concentration is relatively low (as in ref. 7), it may be possible to probe down to the cloud layer with an occultation experiment. This would require sufficient signal power to overcome both refractive defocussing and absorption. The former produces between 20 and 30 dB loss at the cloud layer (ref. 14) and the latter about 30 dB at S-band. Below the cloud layer, the absorption increases much more rapidly than defocussing so absorption would dominate. Above the cloud layer, the absorption would be the lesser of the two.

F. SUGGESTED DUAL FREQUENCY OCCULTATION EXPERIMENT

Finally, the measurements of the ammonia absorption coefficient suggest the use of this data to probe the ammonia distribution. For example, if temperature and pressure were known and refractive defocussing unimportant (as might be the case for a descending probe) then the loss of signal would be correlated with the ammonia concentration.

A second possibility would be to use two different frequencies in an occultation experiment (say X-band and S-band). The refractive defocussing is independent of frequency but the absorption loss is proportional to ν^2. Therefore the total loss could be broken up into absorption and defocussing. Let D = defocussing loss and $A = B\nu^2$ = absorption loss. Then

$$L_1 = A_1 + D = B\nu_1^2 + D$$

$$L_2 = A_2 + D = B\nu_2^2 + D$$

(all quantities are in dB). By measuring L_1 and L_2 and using the known values of ν_1 and ν_2, B and D can be determined unambiguously. From D the pressure, temperature, and composition can be determined as Kliore et al (ref. 17) have done for Venus. Given these parameters and B, the ammonia distribution can be determined according to Eq. (19).

G. SUMMARY

In conclusion, it appears that absorption phenomena will be important in the planned study of Jupiter. In particular, these studies mean that X-band transmission will probably involve too much ammonia absorption to be useful. Even at S-band, there may be limits placed on occulation experiments by absorption rather than refractive defocussing, depending on how low into the atmosphere it proves possible to probe. It may be possible to probe the ammonia distribution with a dual frequency experiment. This would have important bearing on the interpretation of the infrared spectra.

II. MEASUREMENT OF AMMONIA ABSORPTION AT S- AND X-BAND

A. APPARATUS

The absorption coefficient was determined by measuring the change in power transmitted through a cavity when the absorbing gas was admitted. This method gives greater sensitivity than the more obvious one of measuring the power loss along a waveguide. The equipment was kindly supplied by Dr. A. A. Maryott of the National Bureau of Standards. He has described it previously in some detail (ref. 18). Briefly, the power was generated by a klystron operating at 2315 MHz. The frequency was swept over a range of several hundred kHz about the cavity resonance frequency. The power in the cavity was detected with a crystal (assumed square law) and the output applied to the vertical deflection plates of a CRT. The horizontal plates were driven by the klystron frequency modulator signal. Therefore, the mode curve (power versus frequency) of the cavity was displayed on the CRT. Assuming that the energy decay is exponential with time

$$u = u_o \exp - \left(\frac{\omega_o t}{Q_o} + \alpha c t \right) \tag{18a}$$

the mode curve of the cavity has the Lorentz shape [Fourier transform of (18a)]

$$U(\omega) \propto \frac{1}{(\omega - \omega_o)^2 + \frac{\omega_o^2}{4} \left(\frac{1}{Q_o} + \frac{\alpha c}{\omega_o} \right)^2} \tag{18b}$$

See (ref. 19). By measuring the height of the mode curve ($\omega = \omega_o$) with and without the absorbing gas one obtains

$$\frac{\alpha c}{\omega_o} = \frac{1}{Q_o} \left[\left(\frac{U_o}{U} \right)^{1/2} - 1 \right] \tag{18c}$$

where U_o is the height when $\alpha = 0$ and $\omega_o = 2\pi\nu_o$. Q_o was approximately 37,600.

In a typical experiment, 100 Torr of NH_3 was admitted to the cavity and the height of the mode curve measured. The foreign gas (H_2, He or mixtures of the two) was admitted and the height remeasured for each of a series of pressures. This gave U_o/U for each pressure. ω_o and Q_o were

determined once for all and α computed according to (18c). All room-temperature measurements were performed at 25.9 $\pm$ 0.5°C. The results for four such experiments, two with hydrogen and two with helium, are shown in Figures 6, 7, 8, and 9. In each case, the smooth curve is a least-squares fit as described below. All together 5 runs were made with pure NH_3, 11 with H_2, 7 with He and 1 with H_2+He. Experiments were performed with 50, 100, and 300 Torr of NH_3. In all cases the results agreed to within the experimental error.

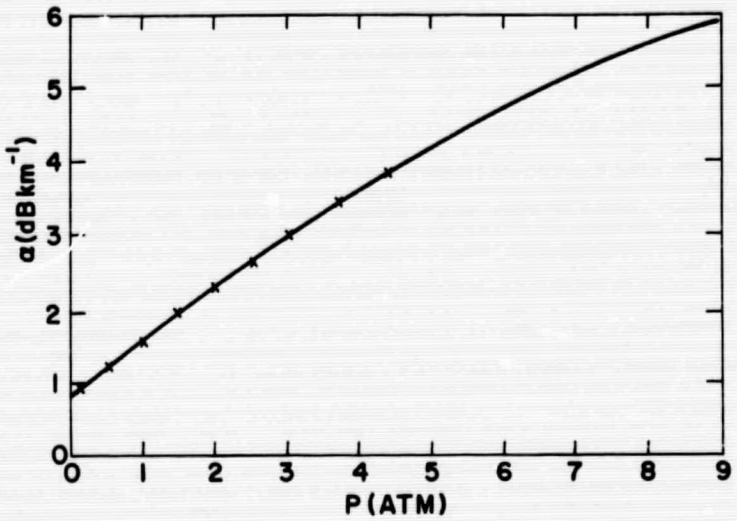

Figure 6. Absorption coefficient versus pressure for 100 Torr of NH_3 broadened by H_2 (2.315 GHz).

TABLE 1

gas	a(MHz Torr^{-1})	b	a+b
NH_3	21.4	14.1	35.5 $\pm$ 4%
H_2	2.5 $\pm$ 10%	1.5 $\pm$ 16%	4.0 $\pm$ 4%
He	(0.8 $\pm$ 10%)*	(0.4 $\pm$ 10%)*	1.1 $\pm$ 10%

*The discrepancy among a, b, and a+b is within its quoted errors. See text.

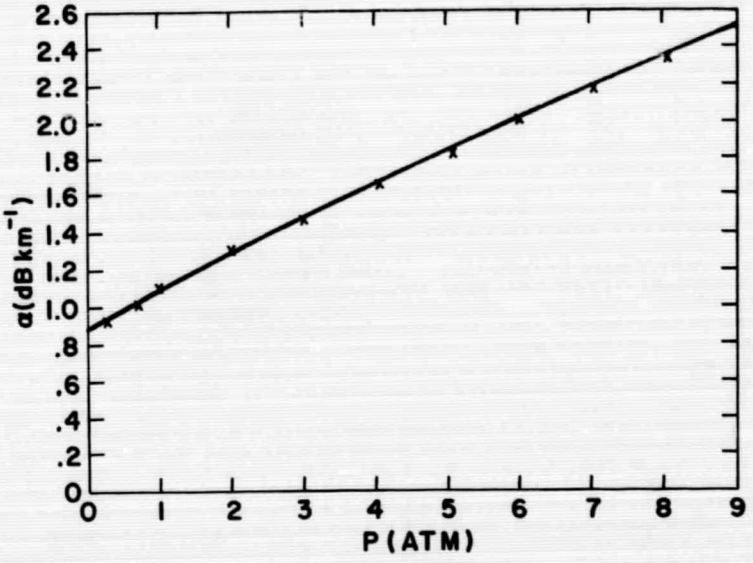

Figure 7. Absorption coefficient versus pressure for 100 Torr of NH_3 broadened by He (2.315 GHz).

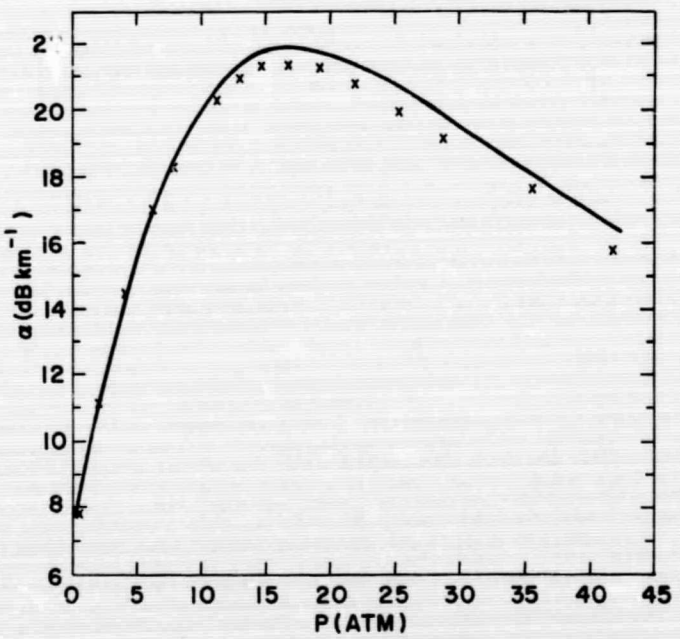

Figure 8. Absorption coefficient versus pressure for 300 Torr of NH_3 broadened by H_2 (2.315 GHz).

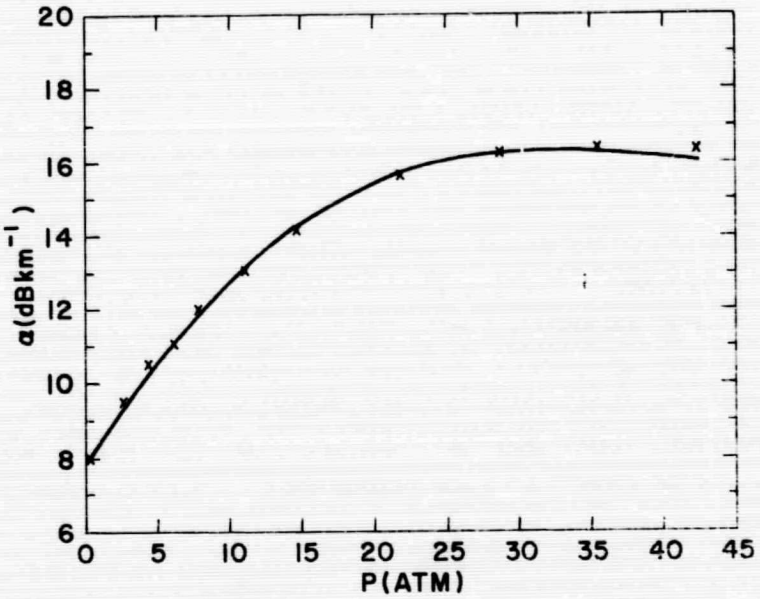

Figure 9. Absorption coefficient versus pressure for 300 Torr of NH_3 broadened by He (2.315 GHz).

B. INTERPRETATION

It was mentioned in Section I.C. on page 5 that the Lorentz expression Eq. (8) is not adequate for a complete interpretation of the data. At the least, there is a contribution due to "negative resonance terms" which has been given by Van Vleck and Weisskopf (see ref. 9). In addition, Ben-Reuven (ref. 10) has pointed to the need to account for those collisions which induce a change in the molecular state. The other theories assume that state changes are only caused by the incident radiation. Ben-Reuven's result is

$$\alpha(\nu) = \frac{\pi}{3c\ kT\varepsilon_o} N\nu^2 \sum\left[f_i |\mu_{ij}|^2 F_i(\gamma_i, \zeta_i, \nu_i, \nu)\right]$$

$$F_i = \frac{2(\gamma_i - \zeta_i)\nu^2 + 2(\gamma_i + \zeta_i)\left[(\nu_{ij} + \delta_i)^2 + \gamma_i^2 - \zeta_i^2\right]}{\left[(\nu_{ij} + \delta_i)^2 - \nu^2 + \gamma_i^2 - \zeta_i^2\right]^2 + 4\nu^2\gamma_i^2} \tag{19}$$

where all symbols have the same meaning as in Eq. (8). If we again choose average values for γ and ν_o:

$$\alpha(\nu) = \frac{\pi}{3c\ kT\varepsilon_o} N\nu^2\ F(\gamma, \zeta, \nu_o, \nu) \sum f_i |\mu_{ij}|^2$$

The Van Vleck-Weisskopf expression mentioned above is obtained by setting $\zeta = 0$ (ζ is a frequency which like γ is proportional to N_S; δ is the shift in resonance frequency. δ may be neglected for pressures below 100 atm).

All of our data were analyzed by fitting them with Eq. (19). The parameters a and b ($\gamma = aP$, $\zeta = bP$) obtained in this way are given in Table 1. In the parameter range of interest the gross properties of Eq. (19) can be obtained by assuming $\nu \to 0$, $\nu_o >> \gamma$ and $\nu_o >> \zeta$. Then

$$F(\nu) \cong 2\,\frac{\gamma + \zeta}{\nu_o^2} = 2\,\frac{a + b}{\nu_o^2}\,P \tag{20}$$

Therefore the limiting slopes in Figs. 6 and 7 give (a+b). One can do somewhat better than this as it is clear that deviations from linear behavior occur. However the deviations are not large so a+b will be given with more precision than a or b separately. A computer least-squares analysis was carried out in which values of a and b were chosen and the absorption calculated. A "penalty function" PF was then formed equal to the sum of the squares of the differences between the calculated and observed absorption for each data point. The "best" values of a and b were those which minimized PF. In addition, an indication of the possible error was obtained from the expected error in PF. a and b were varied until PF became as large as the expected error in PF. The results are shown in Table 1. In the case of NH_3, the data were sufficient to give only a+b without any separation. Therefore b/a = 0.655 was taken from Ben-Reuven (ref. 10) and our value of a+b utilized to obtain a and b.

For He, a and b could only be separated at high pressures where the use of average values of γ and ζ is not expected to be as accurate. However, similar calculations made with the H_2 where a and b could be separated give results which agreed to within the experimental precision. Also note that in Figs. 7 and 10 better fits to the data were obtained with a_{He} = 0.7 MHz Torr^{-1} and b_{He} = 0.3 MHz Torr^{-1}. These values were used in computing Fig. 2.

C. JOVIAN MIXTURES

To show that the results already cited agree with gas mixtures like those found on Jupiter, an experiment was done with NH_3 pressure broadened by H_2 and He. The only other important constituent of the atmosphere (methane) is far too dilute to affect the NH_3 absorption. The result is shown in Fig. 10. The smooth curve was calculated using the parameters in Table 1, and taking

$$\gamma = a_{NH_3} P_{NH_3} + a_{H_2} P_{H_2} + a_{He} P_{He}$$

$$\zeta = b_{NH_3} P_{NH_3} + b_{H_2} P_{H_2} + b_{He} P_{He}$$

where the P's are partial pressures. The agreement is very good which means that any Jovian mixture can be treated in the same way, namely by considering each broadening gas separately.

D. TEMPERATURE DEPENDENCE

Another important property is the temperature dependence of the absorption. Referring to Eq. (19) it can be seen that there is an explicit T^{-1} dependence, a possible temperature dependence in the sum $\Sigma f_i |\mu_{ij}|^2$, and a possible temperature dependence in γ and ζ. We have measured the absorption coefficient at three temperatures 25.9°C, 63.9°C, and 115°C. In analyzing these data, the sum $\Sigma f_i |\mu_{ij}|^2$ was assumed constant and the quantities a and b were determined as previously. These results are shown in Fig. 11. For pure NH_3, $a_{NH_3} + b_{NH_3}$ was proportional to T^{-1} as had been found previously (ref. 21). However, this is difficult to establish with great precision because the temperature range available was rather small. Therefore in computing the coefficients a and b for H_2 and He, the ammonia coefficients were taken strictly proportional to T^{-1}. The hydrogen coefficients were found to be proportional to $T^{-0.6}$ and the helium coefficients proportional to $T^{-0.7}$. The absorption at Jovian temperatures was calculated on the assumption that these laws hold.

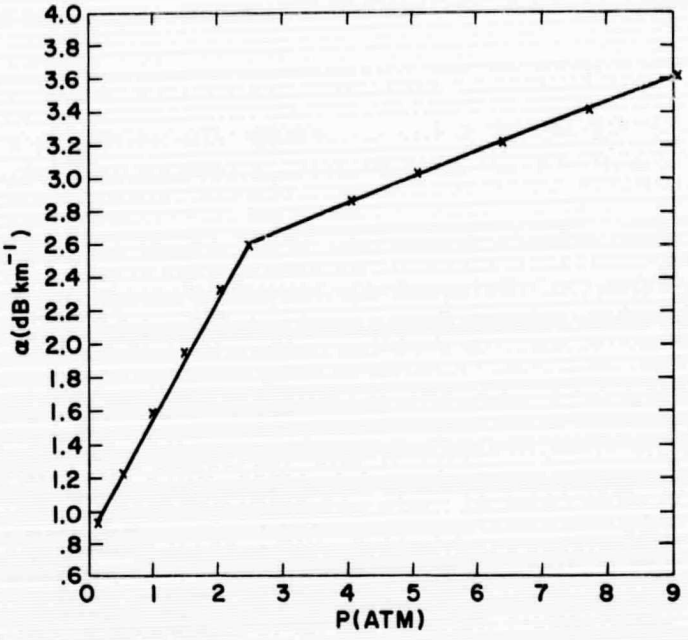

Figure 10. Absorption coefficient versus pressure for 100 Torr of NH_3 broadened by H_2 to 2.49 atm followed by He.

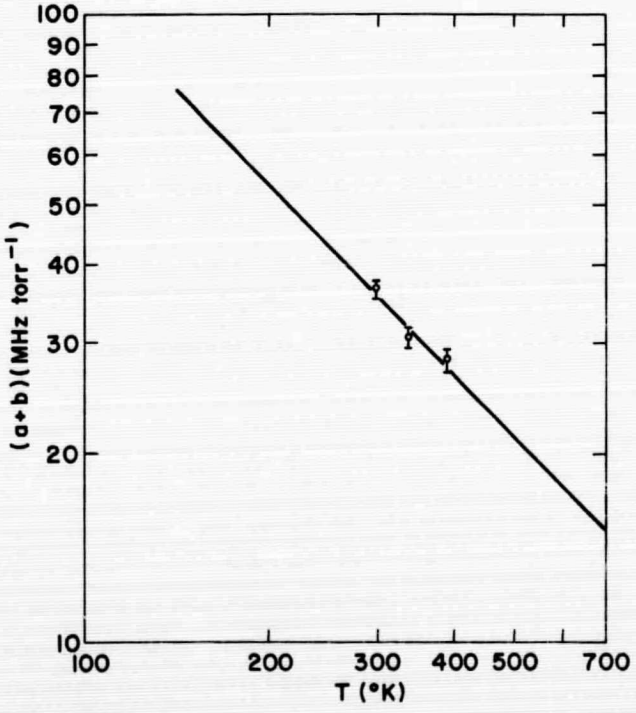

Figure 11(a). Broadening parameter a+b versus temperature for NH_3.

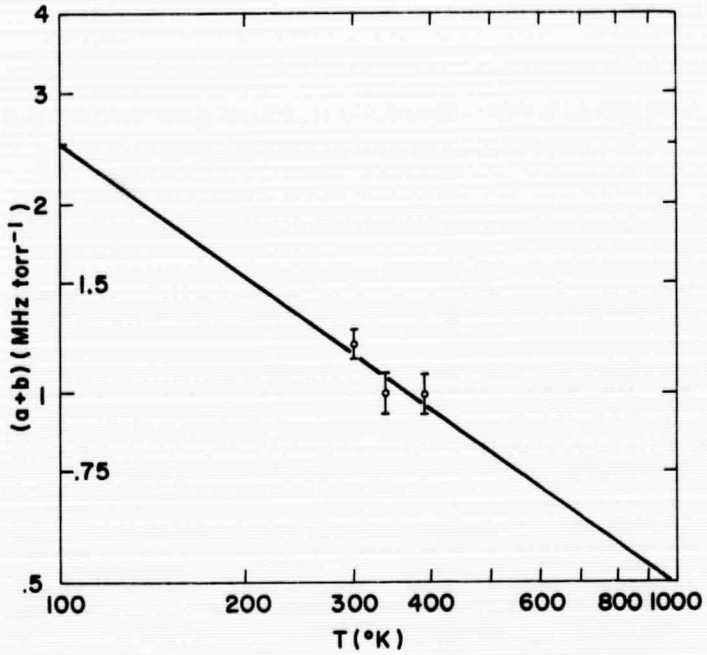

Figure 11(b). Broadening parameter a+b versus temperature for He.

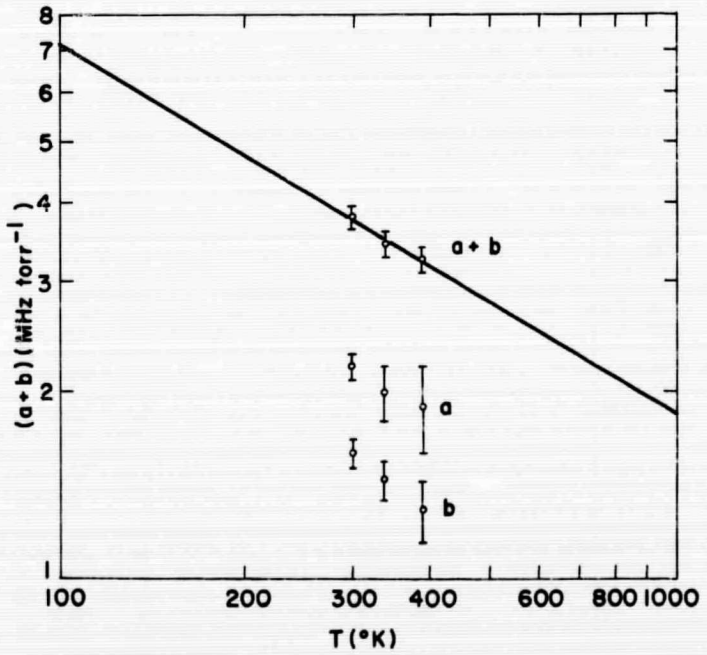

Figure 11(c). Broadening parameter a+b versus temperature for H_2.

E. OTHER FREQUENCIES

Recently, Morris and Parsons (ref. 22) have measured the microwave absorption of ammonia in mixtures of H_2 and He at X-band (9.58 GHz). They were primarily interested in higher pressures and have extended the measurements to several hundred atmospheres. These data are clearly relevant to the Jovian communications problem and will therefore be analyzed in the light of our own.

The most obvious method of comparison would be to calculate the absorption at 9.58 GHz using our values of a and b from Table 1 and compare them with the experimental values. This is shown in Fig. 12. It can be seen that the agreement is quite good for pressures below 25 atm. At the higher pressures there is a discrepancy of about 15% but this is still within the experimental and computational errors.

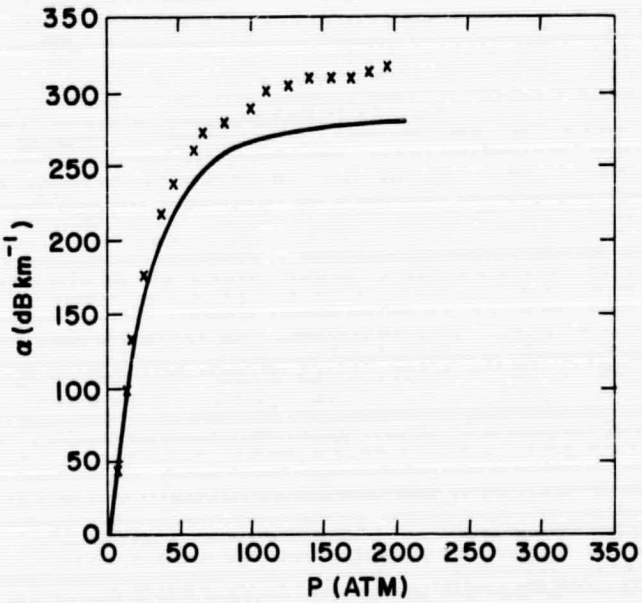

Figure 12. Absorption coefficient versus pressure for NH_3 plus H_2 in ratio $[NH_3]/[H_2] = 1/128$ (9.58 GHz). Data from Morris and Parson's (ref. 22), curve calculated using parameters in Table 1.

However, this procedure is not completely valid because of the nature of the averaging implied by Eq. (19). In particular, the replacement of F_i by a common "average" line shape has the disadvantage that averages of combinations of γ and ζ are achieved rather than averages of γ and ζ separately. For example, in the high-pressure low-frequency

limit, the absorption is determined by $\sum f_i |\mu_{ij}|^2 \frac{1}{\gamma_i - \zeta_i} \neq \frac{1}{\bar{\gamma}_i - \bar{\zeta}_i}$. Here $\bar{\gamma}_i \equiv \sum f_i |\mu_{ij}|^2 \gamma_i$ and $\bar{\zeta}_i$ similarly. In the low-pressure, low-frequency limit, the absorption is determined by $\sum f_i |\mu_{ij}|^2 (\gamma_i + \zeta_i)$ so in this case one *does* obtain true average values of γ and ζ. However, the agreement is within the experimental error anyway, and therefore sufficiently accurate to use our parameters a and b in this way. We can therefore construct the curve Fig. 2 which gives the complete frequency dependence for a point near the cloud layer.

F. WATER VAPOR

It has been mentioned several times that the water-vapor absorption is expected to be much less than the ammonia absorption at least above the cloud layer. A rough indication of this is contained in Fig. 2 where the H_2O absorption coefficient for *Earth* is shown. However a more detailed comparison will now be made.

First, to our knowledge water vapor has not been detected in Jupiter's atmosphere (ref. 7) but has been predicted on the basis of thermodynamic calculations by Lewis (ref. 23). Therefore the distribution with height of the H_2O is uncertain. We will assume that the water vapor is saturated at each temperature. This is a worst-case analysis since in any event no more water vapor could exist in equilibrium.

The microwave absorption spectrum for water vapor consists solely of transitions among the various rotational energy levels of the molecule. There is no "ammonia-like" inversion transition. The line shape for each transition can be computed from the Van Vleck-Weisskopf expression

$$\alpha(\nu) = \frac{8\pi^2}{3c\ kT\varepsilon_o} N\nu^2 \sum f_i |\mu_{ij}|^2 \left[\frac{\gamma_i}{(\nu-\nu_{ij})^2 + \gamma_i^2} + \frac{\gamma_i}{(\nu+\nu_{ij})^2 + \gamma_i^2} \right] \quad (21)$$

Notice that there is an extra factor of 2 in Eq. (21) compared with Eq. (19). This is due to the inversion transition in NH_3 which doubles the number of states, therefore halves the number of absorbing transitions. Eq. (21) has been used by many authors (ref. 16, 24) to analyze the water-vapor absorption; the Ben-Reuven line shape (Eq. 19) does not apply to water vapor.

The lowest transition has a frequency of 22.2 GHz and is the most important for low pressures (less than 1 atm). At higher pressures the higher lines become so broad that they dominate. Ho, Kaufman, and Thaddeus (ref. 24) have studied the water-vapor spectrum when broadened by N_2 at high enough pressures that the 22.2 GHz line may be neglected. They have summarized their results in a formula which in our notation is (ref. 24)

$$\alpha = 6.2 \times 10^{-3} \frac{P_{H_2O} P\nu^2}{(\text{atm})^2 (\text{GHz})^2} \left(\frac{273}{T}\right)^{3.1} \text{dB km}^{-1} \qquad (22)$$

where T is the Kelvin temperature, and P_{H_2O} is the partial pressure of water vapor. P is the total pressure. It might appear that α decreases with increasing T but actually P_{H_2O} rises exponentially with T if we assume the water vapor saturated. Equation (22) is consistent with Eq. (21) because $\nu_{ij} >> \nu$ and $\nu_{ij} >> \gamma_{ij}$. We also recall that $\gamma_{ij} \propto P/T$ and $N \propto P_{H_2O}/T$. The extra factor $T^{0.1}$ comes from a slight additional temperature dependence of γ with T. This formula represents only part of the H_2O absorption at pressures of a few atmospheres or less. Assuming T = 273°K and P = 2 atm with the water-vapor saturated ($P_{H_2O} = 6 \times 10^{-3}$ atm) we obtain (for ν = 2.315 GHz)

$$\alpha \cong 4 \times 10^{-4} \text{ dB km}^{-1}$$

To this must be added the absorption due to the 22.2 GHz line. This has been treated for *Earth* by Van Vleck (ref. 16). He also uses Eq. (21) but with ν_{ij} = 22.2 GHz and $\gamma \cong 3$ GHz. Again, assuming a temperature at the cloud tops of 273°K (a very high value; clearly a worst case) and total pressure 2 atm we find

$$\alpha_{22.2} = 1.3 \times 10^{-4} \text{ dB km}^{-1}$$

Therefore the absorption in this case due to H_2O is $\alpha = 5.3 \times 10^{-4}$dB/km. This is less than 1% of the NH_3 absorption. Further, the water-vapor concentration is almost certainly much less than that assumed (273°K). Therefore, above the clouds, water-vapor absorption may be neglected.

G. SCOPE OF DATA

The significance of section II is that the ammonia absorption coefficients can now be predicted accurately once given a model atmosphere. In particular, these data can be used to calculate ammonia absorption for the region below the cloud layer on Jupiter, for other planets such as Saturn, or for the upper atmosphere of Jupiter as better model atmospheres become available. In short, our ability to predict ammonia absorption below 10 GHz is now limited by the model atmosphere, not the ammonia absorption coefficient.

III. DECIMETRIC RADIATION FROM JUPITER'S ENVIRONMENT

A. GENERAL COMMENTS

In Phase I, a start was made in estimating the effect of radio noise in the low GHz-frequency band envisioned for the communications links with space probes to be sent out to Jupiter and its environments (ref. 25). Figure 7 of ref. 25 is reproduced here as Fig. 13 to stress again that there appear to be two unusual non-thermal sources of noise in the

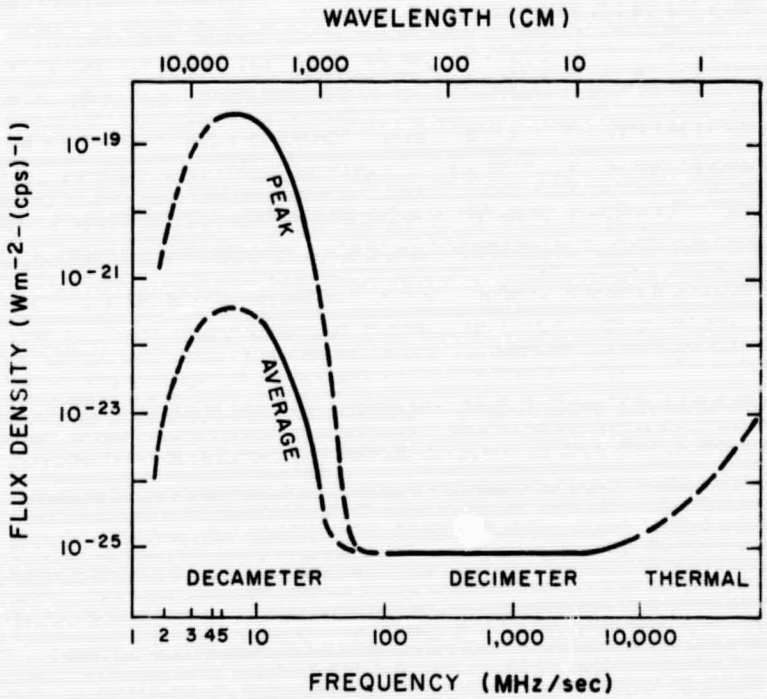

Figure 13. Spectrum of radio frequency radiation from Jupiter's environment (ref. 25).

Jupiter environment: a decameter-wavelength source of strength up to 10^{-19}W/m^{2}Hz, and a source yielding a flat decimeter-wavelength spectrum at a strength of $\sim 10^{-25}$W/m^{2}Hz.

The decametric radiation at the low-frequency end, and the thermal radiation above 20 GHz need not concern us too much. The above quoted flux per Hz for decimetric radiation represents an unusually intense

source of radio noise in the Jovian environment. It points to the possibility of very serious noise interference at the communication frequencies of interest on links including a space probe in the vicinity of Jupiter. As pointed out previously (ref. 25) receivers on earth will be able to cope with such noise, but simple inverse-square-distance scaling yields much higher noise levels, perhaps insurmountable ones, for space probes in the Jovian environment. Close to Jupiter, however, the noise source may no longer be sufficiently localized to allow such scaling. Because it is crucial to the communication problem to estimate the noise interference for such situations - particularly when rough scaling indicates a formidable problem - it will be necessary to review in some detail the nature of the source.

It appears from the analyses reported in the literature (ref. 4) that (relativistic) synchrotron radiation or (non-relativistic) cyclotron radiation are the only mechanisms that can explain the observed radiation characteristics: of these two, cyclotron radiation is rejected because it requires the presence of an abnormally strong magnetic field.

B. ELEMENTS OF SYNCHROTRON-RADIATION MECHANISM

The basic mechanism of cyclotron radiation is well understood. Electrons are trapped by magnetic fields into helical orbits around the field lines with Larmor radii $r_c = mv/eB$ (MKS units for charge e and magnetic field B; v is the tangential velocity). Such a spiralling electron is equivalent to a negative charge oscillating at frequency $\nu_c = v/2\pi r_c$ (or angular frequency $\omega_c = v/r_c = eB/m$) around a relatively immobile positive charge (much heavier, therefore less mobile). The radiator is therefore an oscillating dipole with moment $p = -er_c$, and the radiation field of an oscillating dipole is given in any EM textbook, e.g., in Stratton (ref. 26). Synchrotron radiation is only the extension of the same principles to relativistically spiralling electrons. One finds for the radiated power in all directions

$$P = \frac{\omega_s^4 (er_s)^2}{6\pi \varepsilon_o c^3} \gamma^4 \qquad (23)$$

in complete analogy (except for the factor γ^4) with non-relativistic effects. Here, $\omega_s = eB/m\gamma$ and $r_s = \gamma mv/eB$ with the relativistic parameter $\gamma = (1-v^2/c^2)^{-1/2}$. The radiation from a relativistic electron at velocity v differs from cyclotron radiation in two major respects: the power P is spread over a frequency interval around ω_s of width $\Delta\omega \sim \gamma^3\omega_s$, and the directions of radiation are concentrated in the plane perpendicular to the B-field, with an angular spread $\Delta\theta \sim \gamma^{-1}$ outside of this plane.

These facts hold for one electron circling with constant relativistic tangential velocity v around a magnetic field line. The hypothesized situation in Jupiter's environment can be regarded as an aggregate of many electrons spiralling at different velocities and pitch angles around the field lines of a magnetic dipole off-centered in the planet (ref. 27). Blumenthal and Gould (ref. 28) give an expression for $P(\nu,\gamma)$, the power of frequency component ν for one electron with its velocity defined by γ

$$P(\nu,\gamma) = \frac{\sqrt{3}\, e^3 B}{4\pi\, \varepsilon_o mc} \frac{\nu}{\nu_o} \int_{\nu/\nu_o}^{\infty} d\xi\, K_{5/3}(\xi), \qquad \nu_o = \frac{3\omega_s}{4\pi} \gamma^3 \tag{24}$$

where $K_{5/3}$ is a Bessel function. Assuming an electron distribution over velocities, $N(\gamma) = N_o \gamma^{-p/4\pi}$, they arrive at an expression for the radiated power at frequency ν from a distribution of electrons after integrating over all velocities. The result is

$$P_N(\nu) = N_o \frac{e^3 B}{\varepsilon_o mc} \left(\frac{3\nu_o}{\nu}\right)^{(p-1)/2} a(p), \tag{25}$$

with $a(p)$ a weak function of p. The observed spectrum is flat, leading to the choice $p \approx 1$ and $a(p) \approx 0.3$ in Eq. (25).

C. APPLICATION TO JUPITER'S ENVIRONMENT

The preceding formulation ignores certain subtleties such as the distribution of pitch angle α (α is a measure of the ratio of velocities normal and parallel to B), and the curvature of field lines. Chang and Davis (ref. 29) have taken these into account and performed computer calculations for a Jupiter-like situation. The resulting flux and power levels as functions of viewing angle with respect to the magnetic-dipole source are not easily applied to the situation we have in mind unless we are prepared to evaluate a number of complicated double integrals. It is our opinion that this is not worthwhile in view of the uncertainties and the many approximations required. Moreover, inspection of Chang and Davis' tables of results reveals only minor variations (well within 10 dB for most of the chosen parameters) of the computed quantities. We shall therefore proceed with a simpler, more approximate model that has much greater flexibility.

Two experimental observations of decimetric radiation from Jupiter are available:

(1) The flux density received on Earth per Hz is $\sim 10^{-25}$ W/m^{2}Hz and it yields a relatively flat spectrum between 100 MHz and 20 GHz.

(2) The angular extent of the emitter appears to correspond to a region extending 3 Jupiter diameters (6 R_J) in the equatorial plane and 1 diameter (2 R_J) in the polar direction (Jupiter's equatorial plane does not deviate appreciably from the ecliptic - the deviations are felt as modulations of the received flux as a function of Jupiter's position in its revolution around the sun).

A sketch of several magnetic field lines of Jupiter intersecting the equatorial x - 0 plane at $r_E \approx 3\ R_J$ is given in Fig. 14. The Earth

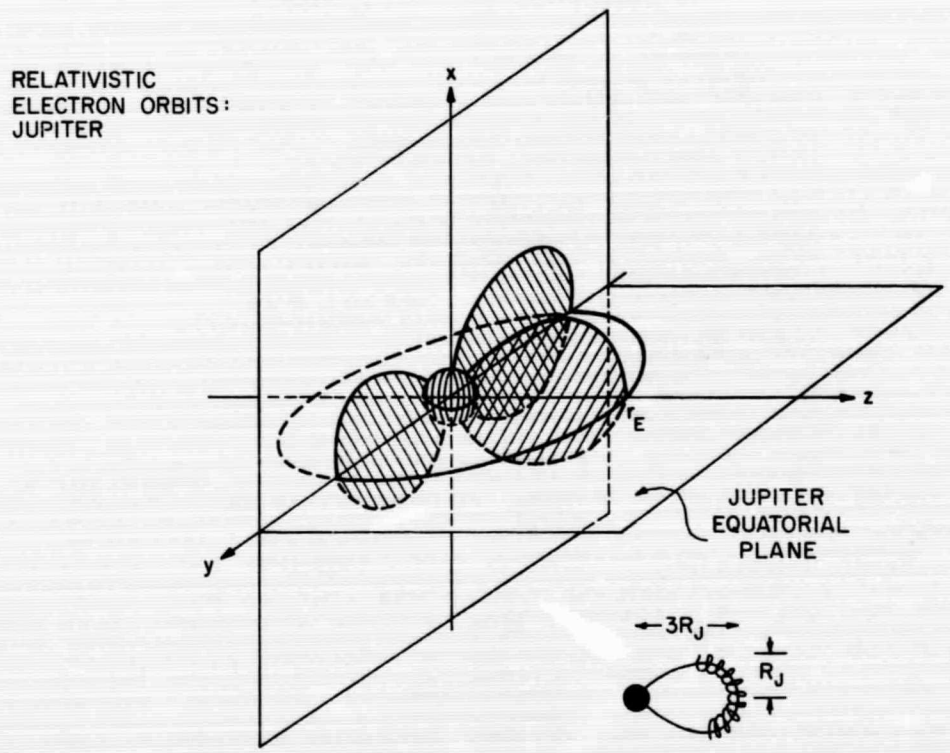

Figure 14. Synchrotron-radiating electron orbits around magnetic field lines: geometry.

is considered to be in the + z direction. A simplified picture of synchrotron radiation received on Earth is obtained by considering contributions only from electrons with Larmor orbits in a plane parallel to the z axis. This approximation assumes with some justification that the

γ^{-1} angular deviation from the preferred direction is small compared to field-line curvature effects. All electrons spiralling around field lines in the z = 0 plane contribute. Those electrons spiralling around field lines in the y = 0 plane contribute only when they cross the x = 0 plane. A complicated volume factor for contributing electrons ensues, which we will estimate shortly.

In order to estimate noise in the Jovian environment, the observed flux density on Earth must be translated into power emitted by electrons in Jupiter's magnetic environment. Let $S_o \approx 10^{-25} W/m^2 Hz$, and R_o be the Earth-Jupiter distance ($R_o \sim 6 \times 10^{11} m$). An equivalent isotropic emitter would radiate $P_J(\nu) = 4\pi R_o^2 S_o$ W/Hz in all directions. The picture of Fig. 14 indicates that the deviation from isotropy is not significant, so that this is perhaps a reasonable approximation of the power per Hz emitted through synchrotron radiation. We equate it to an integral

$$P_J(\nu) = \int dV \quad (dP_N/dV) \tag{26}$$

and interpret the right-hand side of Eq. (25) as dP_N/dV provided N_o is a density. Constant electron density can be expected along a magnetic-flux tube with volume element (ref. 29)

$$dV \sim r_E^2 \sin^7\theta d\theta d\phi dr_E, \tag{27}$$

where dV is centered at r_E,θ,ϕ (in polar coordinates applied in Fig. 14). Interpreting $dP_N(r_E,\theta,\phi) = dV\ (dP_N/dV)$ we multiply Eqs. (25) and (27) to obtain

$$dP_N \approx N_o B_E \frac{e^3}{\varepsilon_o mc}\ 0.3\ (1 + 3\cos^2\theta)^{1/2} \sin\theta d\theta d\phi r_E^2 dr_E, \tag{28}$$

where we have scaled $B(r_E,\theta,\phi)$ to $B_E = B(r_E,0,0)$ by means of well-known magnetic-dipole behavior. It appears that $r_E \sin\theta \lesssim R_J$, i.e. $\sin\theta < 1/3$, consequently the angle-dependent square-root factor in (28) hardly differs from 2. The remaining $\sin\theta d\theta d\phi r_E^2 dr_E$ is just the volume element at (r_E,θ,ϕ) and it integrates out to the total effective volume V. Michaux (ref. 4) and Moroz (ref. 5) estimate V $\sim$ 10 times Jupiter's volume $\sim 13\pi R_J^3$. We believe this to be high. The area inside the $3R_J$ magnetic contour is $12r_J^2/5$ and the toroidal shape obtained by multiplying by $2\pi r_E = 6\pi r_J$ is certainly too large in view of the unfavorable

aspect of such contours in or close to the y = 0 plane as well as due to shielding by the planet of a portion of the radiating electrons from Earth. Instead of $13\pi R_J^3$, we use $6\pi R_J^3 \sim 7 \times 10^{24} m^3$ as a volume estimate. Thus we obtain, using $e^3/\varepsilon_o mc \approx 1.5 \times 10^{-24}$ (MKS units).

$$P_N \sim N_o B_E \times 3.5 \text{ W/Hz} \tag{29}$$

We equate this to $P_J = 4\pi R_o^2 \times 10^{-25} \sim 0.45$ W/Hz to obtain,

$$(N_o \text{ in } cm^{-3}) \quad (B_E \text{ in gauss}) \approx 10^{-3} \tag{30}$$

This constraint is within a factor 2 of the criterion quoted by Michaux from data by Chang and Davis (ref. 29). It reaffirms the hypothesis that our simplifying assumptions are sufficient. Moroz (ref. 5) obtains a value for N_oB that is an order of magnitude higher but there appear to be several errors in his estimate. Clarke (ref. 30) in an updated version of the Chang and Davis calculations finds an N_oB value somewhat more than an order of magnitude lower than Eq. (30). Clearly, agreement is imperfect, and the inaccuracies we introduce through simplifying the model must therefore be inconsequential.

We utilize our approximate value of $P_J \sim 0.45$ W/Hz together with our estimate of volume V to obtain an estimate of the power radiated per unit volume per Hz:

$$dP_N/dV \sim 6.4 \times 10^{-26} W/m^3 Hz \tag{31}$$

D. EARTH-TO-PROBE COMMUNICATIONS

Although the flux per Hz impinging upon Earth from Jupiter's relativistic electrons is low $\sim 10^{-25}$ W/m^2Hz, inverse-square distance scaling indicates a possible noise problem in Earth transmission to a probe on a mission towards Jupiter. We consider a number of cases in reference to the situation depicted in Fig. 15.

1. Probe Not Close to Jupiter ($R_2 >> 3R_J$)

For situations in which a space probe on its way to Jupiter is still fairly distant from the planet ($R_2 >> 3R_J$) inverse-square-distance scaling

PROBE NOT CLOSE TO JUPITER

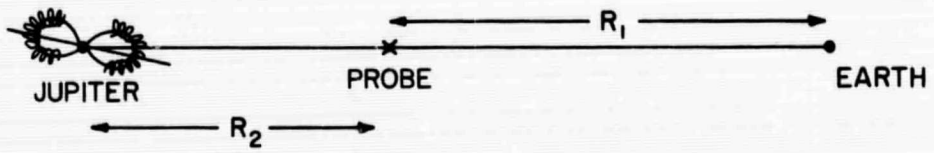

Figure 15. A probe enroute to Jupiter.

of Eq. (31) is sufficient. We set $P_N = (dP_N/dV)\ V \sim 0.25$ W/Hz to obtain a noise flux at the probe of $S_N = P_N \Delta\nu/4\pi R_2^2$ where $\Delta\nu$ is the bandwidth of the receiver. The flux from an earth-based transmitter is $S_e = P_e G_e/4\pi R_1^2$ where P_e is the total power available from the transmitter and G_e is the antenna gain. Taking a factor $K_p^{-1}(K_p>1)$ to account for directional shielding of Jovian noise entering the probe receiver from directions other than that of signals from earth we note that $S_e > S_N$ (i.e., signal-to-noise ratio is larger than unity) when

$$P_e > 0.45\ \Delta\nu\ G_e^{-1} K_p^{-1} R_1^2/R_2^2 \quad W \tag{32}$$

2. Probe Close to Jupiter ($R_2 \lesssim 3R_J$)

When the probe approaches the $3R_J$ distance to Jupiter, and enters into the noise-generating region, it will be clear that the R_2^{-2} scaling of noise power can no longer be trusted because the noise region is no longer a point source. Many of the approximations made previously break down. Consider Fig. 16, and the noise emanating from a magnetic field line at angle α with that in the y = 0 plane, specifically from a location at distance r_α from the probe (which is on the z-axis). Let $\vec{r}$ be the vector from Jupiter to that location so that the probe location $\underset{\sim}{r}_p = \underset{\sim}{r} - \underset{\sim}{r}_\alpha$. The noise flux from volume element $dV = (r^3/r_E^3)d^3r$ [see Eq. (27)] due to electrons with velocity γ is

$$dS_N(\nu) = \int d\gamma\ \frac{N(\gamma)\ P(\nu,\gamma)\ f(\vec{r}_\alpha,\gamma)}{4\pi r_\alpha^2}\ \frac{r^3 d^3 r}{r_E^3} \tag{33}$$

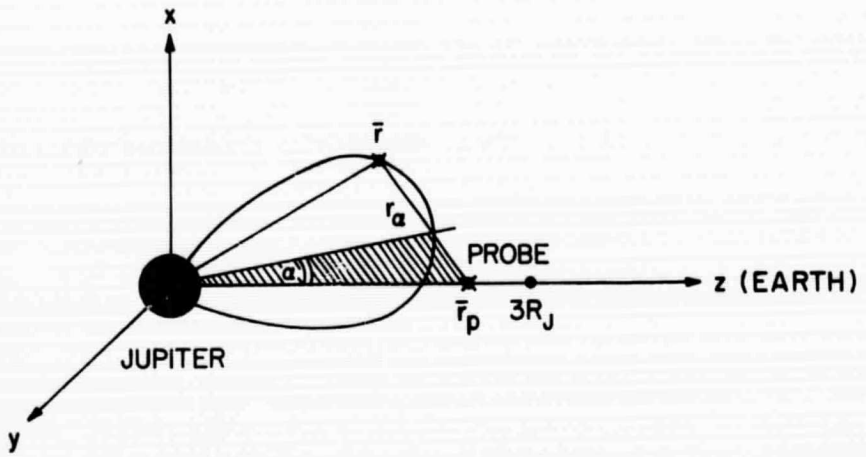

Figure 16. A probe within the $3R_J$ distance of Jupiter. (α is an angle in the yz plane.)

where $f(\vec{r}_\alpha,\gamma)$ is a polarization factor describing the fraction of energy at velocity γ radiated into the probe from dV at $\vec{r}$ (when γ is large, f will be small unless the electron orbit and the probe lie in - or near to - the same plane). When $r_\alpha = |\vec{r}-\vec{r}_p|$ becomes very large compared to $3R_J$, Eq. (33) reduces to $dP_N/4\pi R_2{}^2$ with dP_N given by Eq. (28). As complicating factors, we must now deal with $f(\vec{r}_\alpha,\gamma)/r_\alpha{}^2$ in Eq. (33). It can be seen from Eq. (24) that $P_N(\nu,\gamma) \propto X^{-1/2}\exp(-X)$ for $X > 1$ ($X = \nu/\nu_o$, therefore $X \propto \gamma^{-3}$ in this application). Therefore, except for extremely high values of γ, we have $P_N(\nu,\gamma) \propto \gamma^{3/2}\exp(-\gamma^{-3})$. Because $N(\gamma) \propto \gamma^{-1}$ we observe that $N(\gamma)P_N(\nu,\gamma) \propto \gamma^{1/2}/\exp(\gamma^{-3})$. Except for $\gamma \sim 1$, we see that $N(\gamma)P_N(\nu,\gamma) \propto \gamma^{1/2}$ i.e., is weighted towards large γ (as long as γ is not so large that $\nu/\nu_o \lesssim 0.3$ in which case $P_N \to 0$ rapidly). However, at large γ, the $f(\vec{r}_\alpha,\gamma)$ factor will be appreciable only for a range of angles $\sim \gamma^{-1/2}$ around the location $\vec{r}$ where the electron orbits lie in a plane intersecting the probe. Most of the contribution to Eq. (33) appears to come from large $-\gamma$ electrons, i.e. from locations on each magnetic contour at angle α close to the "perpendicular" locations. Having made this point, we need look only at those locations $\vec{r}$ for which $\vec{r}_\alpha$ lies nearly in the plane of electron orbit (on each magnetic contour line there are at most two such locations).

Even so, the geometry is complicated and it is a horrendous job to evaluate Eq. (33) accurately. However, we note that $r^3 < r_E{}^3$, and that $d^3r/r_\alpha{}^2$ integrates to a length also less than r_E (the factor $f(\vec{r}_\alpha,\gamma)$ restricts the size of d^3r). Therefore, a saturation effect occurs and we can set $d^3r(r^3/r_E{}^3)f/r_\alpha{}^2 \approx 12\pi\beta R_J$ with $\beta < 1$, a constant to be

fitted appropriately. This procedure makes $S_N(\nu)$ independent of probe location, which it really is not, but the above line of reasoning appears to indicate that dS_N varies only weakly with probe location once the probe is inside the $3R_J$ region. Consequently, we obtain as an approximation:

$$S_N(\nu) \sim 3\beta R_J (dP_N/dV) \tag{34}$$

The total noise flux is $S_N = S_N(\nu)\Delta\nu$, and we will include a factor K_p^{-1} (inverse gain at the probe) to indicate possible shielding out of some of the noise. Thus $S_N = 3K_p^{-1}\beta R_J(dP_N/dV)\Delta\nu$ is compared to $S_e = P_e G_e/4\pi R_1^2$, and in order that the ratio S_e/S_N exceeds unity we must have

$$P_e > 10^7 \Delta\nu \beta^{-1} (G_e K_p)^{-1} \quad W \tag{35}$$

In Eq. (35) we have used $r_E = 3R_J \approx 2.1 \times 10^8$m and $R_1 \approx 6 \times 10^{11}$m ($R_1$ is fairly constant when $R_2 \lesssim 3R_J$). We shall fit the value of β by making $S_N = 3\beta R_J(dP_N/dV)\Delta\nu$ a saturation level for $S_N = V(dP_N/dV)\Delta\nu 4\pi R_2^2$ when R_2 decreases to $3R_J$. Setting $3\beta R_J = V/4\pi R_2^2$ at $R_2 \sim 3R_J$ we obtain $\beta^{-1} \approx 20$. This would also have been obtained by scaling the R^{-2} isotropic radiation law to $R \approx 3J$. The saturation noise flux per Hz is therefore of the order $dS_N/d\nu \sim 10^{18}$W/m^{2}Hz.

3. Some Numerical Results

We can summarize Eqs. (32) through (35) by means of a simple interpolation formula:

$$S_e/S_N \sim \left[10^7\beta^{-1} + 4R_2^2/R_1^2\right] G_e K_p P_e/\Delta\nu \qquad \beta^{-1} \sim 20 \tag{36}$$

When $R_2 < 3R_J$, the $10^{-7}\ \beta^{-1}$ contribution dominates, when $R_2 >> 3R_J$ it is the other term in Eq. (36) which determines the signal-to-noise ratio. Let us apply Eq. (36) to an up-link communication with a probe in the $3R_J$ region. Because much of the noise comes from directions close to that of the signal from Earth, and/or because shielding out of such noise may not be possible we expect $K_p \sim 1$. Let us furthermore assume

we have the 85-ft. Deep Space antenna at Goldstone as a transmitter. Then, $G_e \sim 10^5$ and $P_e \sim 10^4$W. Applying Eq. (36) for diverse communication bandwidths $\Delta\nu$ we obtain:

TABLE 2

$\Delta\nu$ in Hz	S_e/S_N in dB
10^3	3
2×10^3	0
10^4	-7

The above values can be scaled to other system parameters by using Eq. (36); furthermore the value $\beta^{-1} \sim 20$ may be in error by 3 dB or so.

E. PROBE-TO-PROBE COMMUNICATIONS

Another potentially interesting situation is that of two probes in Jupiter's environment which attempt to maintain a communications link between them. Since both power transmission and gain factors must be much less than an Earth-based radar, it is not clear that the much reduced propagation distance will enable a probe transmitter to overcome the synchrotron-radiation noise received by the other probe. Consider probe 2 within the $3R_J$ radius, and probe 1 (with the transmitter) at any location. The noise flux received by probe 2 is $S_N = S(\nu)\Delta\nu$ as given in Eq. (34). The flux received by probe 2 from the transmitter on probe 1 is $S_{12} = P_1/4\pi R_{12}^2$ (the gain factors are of the order of unity because probe transmitter and receiver should be fairly isotropic). The signal-to-noise ratio is

$$S_{12}/S_N = 2.5 \times 10^{16} P_1/\beta\Delta\nu R_{12}^2 \qquad (37)$$

with P_1 in W, $\Delta\nu$ in Hz, and R_{12} in m. As an estimate, we assume $P_1 \sim 50$ W, $\Delta\nu \sim 10^4$Hz, and $\beta^{-1} \sim 20$. These assumptions yield the rather startling information that the signal-to-noise ratio decreases below unity *when the interprobe distance R_{12} exceeds 10,000 km.* This critical distance

scales with $(P_1\beta^{-1}/\Delta\nu)^{1/2}$, and, therefore, appears to be estimable without gross error. As it is much less than $3R_J$, we see that in effect, probe 1 must also be within the $3R_J$ region.

F. FLUX VS POWER: COMMENTS

In subsections III.D and E. on pages 29 and 33, respectively, we have worked out some numerical results for signal-to-noise-flux ratios. In Section IV on page 35, we shall utilize the results of these flux calculations to estimate the signal powers actually received on board space probes and their satellite probes. Only then can the significance of Jovian noise be evaluated in comparison to internal noise.

IV. CONSEQUENCES FOR JOVIAN TELECOMMUNICATIONS LINKS

The purpose of Phases I and II of this contract has been to identify various sources of radio-wave degradation in planetary environments, and to study their effect upon typical communication links in the 1 to 10 GHz frequency band during space-probe missions. Whereas Phase I was concerned mainly with missions to Venus, the present study has been oriented toward planned missions to Jupiter (such as Pioneer F and G, or future modifications of these). We have discussed each type of radio-wave degradation separately in the preceding sections. In this section, we will discuss how our results affect a hypothetical mission to Jupiter. First, a brief summary of the results is given.

A. FACTORS INFLUENCING PROPAGATION

(1) Turbulence in dense planetary atmospheres induces fading of radio-wave signals. It was shown that the fading can be severe at 2 GHz and higher frequencies when ray paths traverse several kilometers of the lowest 25 km of the Venusian atmosphere (see Phase I final report and Section V of this report on page 41). Although we cannot at this time make a sufficiently accurate statement about fading on Jupiter (see constraint Section IV.B.1 on page 36), we can define a region of Jupiter's atmosphere where appreciable fading may occur; namely, the 50 to 100 km of upper atmosphere above the cloud layer. Other types of signal degradation are probably more severe for ray paths passing close to or penetrating the cloud layer.

(2) The presence of ammonia in the Jovian atmosphere indicates the possibility of strong signal attenuation due to absorption of electromagnetic energy from signals traversing this region (see Section I on page 1). The estimates are sensitive to the amount of ammonia and the pressures assumed for the Jovian atmosphere. There do not appear to be other atmospheric constituents that absorb appreciable amounts of energy from signals in the 1- to 10-GHz frequency range.

(3) When rays enter an atmosphere with a radially varying refractive index at an angle to the local normal, they are refracted toward the normal. Rays penetrating deeper are refracted more strongly. Therefore a beam of rays is defocussed. As a result of refractive defocussing the signal received at a distance is attenuated. Signal loss may exceed 20 dB for signals traveling tangentially to Jupiter's surface at altitudes of 30 to 100 km above the cloud layer. The loss decreases rapidly with increasing altitude, but is only weakly dependent upon frequency. Our estimates (see Section I on page 11), based upon the work of Kliore, et al. at JPL and Sodek (ref. 14) indicate that pressure-broadened ammonia absorption losses (see Section IV.B.2 on page 36) may be far more important than refractive defocussing in the upper part of the 1- to 10-GHz frequency band.

(4) The Jovian ionosphere appears to contain important noise sources. The sources are relativistic electrons spiralling around Jovian magnetic field lines and emitting highly directed synchrotron radiation having a flat spectrum in the 1- to 10-GHz band. We estimate a noise flux saturating at a value between 10^{-19} and 10^{-18} $Wm^{-2}Hz^{-1}$ at locations closer to Jupiter than three radii. This flux can exceed the signal flux from the Goldstone Deep Space antenna if received-signal bandwidths exceed 1 kHz. The mechanism and some signal-to-noise flux calculations are discussed in Section III on page 24. Even if the synchrotron-radiation mechnism is the correct explanation of the noise source, the density of relativistic electrons remains quite small and does not imply an ionosphere of any significance. The observed *decametric* radiation on the other hand, has been interpreted (somewhat speculatively) as due to ionospheric-plasma oscillations: in this case the densities are hypothesized to be as high as $10^{7}cm^{-3}$ -- somewhat higher than in Earth's F layer. The expectation that ionization rates are lower in a planet (Jupiter) further away from the sun does not necessarily contradict this hypothesis since recombination rates can be lower also.

Discussion of the significance of these results for radio-wave experiments during a future space-probe mission to Jupiter is severely limited by several constraints. The next step is to summarize these constraints.

B. CONSTRAINTS IN APPLICATION OF LOSS FACTOR

(1) Estimates of signal fading in the Jovian atmosphere are highly uncertain because the signal-fading parameter σ_ε^2 can be determined only within a range of two orders of magnitude. The parameter σ_ε^2 for Jupiter can be estimated from the known steady-state properties of its atmosphere and from a deduced value of the ratio of standard deviation of mean refractive-index difference n-1. In the absence of *in situ* measurements, the ratio can be estimated by extrapolating the measured Earth and Venus ratios (the latter are actually deduced from fading measurements) to Jupiter. Unfortunately, the Venus ratio appears to be much higher than the Earth ratio. After our recent revision of the Venera-4 analysis (Section V), it was found that the Venus ratio had been overestimated (but this overestimate did not affect our fading estimates for the Venusian atmosphere seriously). Even so, there is still a discrepancy with the Earth ratio. Therefore we feel it desirable to postpone an estimate of signal fading due to turbulent Jovian atmosphere until less unreliable results can be obtained. This may occur when Soviet Venera-7 data is released.

(2) Although ammonia is an important constituent of the Jovian atmosphere, its role as an absorber of EM energy in the 1-10 GHz frequency range seemed as unimportant initially as that of other atmospheric constituents. Its concentration at the cloud layer appeared to be low and

its lowest absorption line lies well above 10 GHz. Nevertheless, we found from theoretical considerations that pressure broadening of these lines under the hypothesized atmospheric conditions at and under the cloud layer leads to significant signal loss. No data at these pressures corroborating this important theoretical estimate were available. The original work effort was therefore redirected and an experimental program of measuring absorption in a laboratory-simulated Jovian atmosphere was initiated at the National Bureau of Standards facility in Maryland. This was made possible through the cooperation and kind assistance of Dr. A. A. Maryott of that organization. The results of these recently completed measurements have been included in this report (Sections I and Section II, pages 1 and 13, respectively). These results are compared with related data recently reported by other investigators. These basic results are thus quite new, and the effort required to obtain them has constrained our absorption analysis to signal-loss estimates in dB/km for several elementary situations only.

(3) Electrons spiralling around magnetic-field lines at relativistic velocities, U, emit synchrotron radiation in directions that deviate from the plane of the electron orbit by a small angle of order $(1-U^2/c^2)^{1/2}$ radians. This constrains the directions in which noise is received by a receiver in Jupiter's environment (e.g., within 5 radii of the planet). The magnitude of this noise depends crucially upon the electron concentration in these directions and upon the range of velocities. Unfortunately, these two parameters contain large uncertainties. Therefore, detailed predictions of synchrotron noise - e.g., well within an order of magnitude of uncertainty - do not appear to be possible at this stage of the investigation.

C. APPLICATION TO HYPOTHETICAL JUPITER MISSIONS

The constraints given above limit our ability to calculate the effects of the Jovian environment on space craft telemetry systems. Nevertheless, it does appear possible to draw some conclusions about the factors which must be taken into account in the design of realistic communication systems. Let us consider a hypothetical spacecraft as it approaches Jupiter, encircles it (perhaps launching a radiosonde in the process), and then passes beyond the planet, perhaps to be occulted by it.

(1) Approach Period

When the spacecraft is further than several hundred km from the cloud layer, neither absorption nor refractive-defocussing losses, nor signal fading can occur (approximately an atmosphere of pressure is required for appreciable effects). Our studies in Section III on page 24 indicate the possibility of severe noise interference on spacecraft within several radii of Jupiter because the noise sources are relatively close to the spacecraft. They can then compete with the very weakened signals

arriving from Earth. Our considerations were based upon *noise-flux* calculations. Here, we will be somewhat more detailed and consider the *power* received by an on-board antenna.

(a) The flux received from the Goldstone Deep Space 85-ft. dish transmitter is $S_e = P_t/4\pi R^2$, where $P_t \sim 10^4$W, $G_t \sim 10^5$, and $R \sim 5 \times 10^{11}$m. The received flux thus amounts to $S_e \sim 3 \times 10^{-17}$W/m^2. It can be distributed over a chosen bandwidth, of course. The power received on board the spacecraft is

$$P_e = (\lambda^2/4\pi)\, G_r S_e \sim 6 \times 10^{-20}\, G_r \text{ W (at 2 GHz)} \qquad (38)$$

(b) The noise flux per Hz received within several Jovian radii of the planet, $S_N(\nu)$, is given by Eq. (34). We have estimated $S_N(\nu) \sim 10^{-18}$W/m^{2}Hz. The received noise power is therefore

$$P_N = (\lambda^2/4\pi) \int d\Omega\, S_N\,(\nu,\Omega)\,|f(\Omega)|^2 G_r \Delta\nu \qquad (39a)$$

where $f(\Omega)$ is the antenna-pattern of received voltage as a function of the solid angle Ω of reception (ref. 16). We have introduced $S_N(\nu,\Omega)$ as the received flux per Hz from the direction characterized by Ω (its integral over all directions is $S_N(\nu)$),. The angle Ω is defined with respect to the direction of maximal gain G_r (note that $|f(0)| = 1$). Finally, $\Delta\nu$ is the bandwidth of the signal accepted by the receiver. For an *isotropic* antenna, $G_r = 1$ and $f(\Omega) = 1$, and we obtain

$$P_N = (\lambda^2/4\pi)\, S_N\,(\nu)\, \Delta\nu \sim 1.5 \times 10^{-21}\, G_r\, \Delta\nu \text{ W (at 2 GHz)} \qquad (39b)$$

On the other hand, if the receiver is highly directional, and if most of the noise comes from a solid angle within the main antenna-pattern lobe, we can approximate Eq. (39a) by

$$P_N \approx (\lambda^2/4\pi)\, S_N\,(\nu)\, G_r\, \Delta\nu \sim 1.5 \times 10^{-21}\, G_r\, \Delta\nu \text{ W} \qquad (39c)$$

One should take note of the difference between Eqs. (39b) and (39c); the latter yields greater noise power received by the factor G_r The reason for this difference is that the noise source is assumed to lie well within the main lobe so that $|f(\Omega)|^2 \approx 1$ is a good approximation in Eq. (39a). For example, this might be expected to be a reasonable approximation when the receiver is pointed towards that region of the spiralling electrons where their orbits around the magnetic field lie in a plane going through the receiver.

(c) Finally, we take into account internal-receiver noise $P_{NT} \sim kT\,\Delta\nu$, due to irregular voltage fluctuations from receiver components at temperature T (usually of the order of 300°K). Thus,

$$P_{NT} \sim kT\,\Delta\nu \times N.F. \sim 4 \times 10^{-21}\,\Delta\nu \times N.F.\ W \qquad (39d)$$

where N.F. is the noise figure of the receiver. A crucial point in comparing Eqs. (39b,c,d) with each other is that internal set noise is still higher than received Jovian-synchrotron noise at S-band and higher frequencies unless configurations with directional antennas (with at least a gain of $G_r \sim 10$) occur in which most Jovian noise sources lie within the main lobe, or unless the internal receiver noise temperature can be reduced greatly below 300°K.

The question arises whether a directional antenna with a gain $G_r \gtrsim 10$ can then pick up so much Jovian noise in its main lobe that this noise outweighs internal set noise. A dish antenna with diameter D has a gain $G_r \approx \pi^2 D^2/2\lambda^2$. Its beam width is $\theta \sim \lambda/D \sim \pi(2G_r)^{-1/2}$. For $G_r = 10$ we find $\theta \sim 40°$. It appears from the geometry (comparable to that in Fig. 16) that an appreciable fraction of noise sources lie outside of a 20° half angle for any location of the spacecraft in this region. Therefore, uplink communication at this stage of a mission appears to be limited chiefly by internal set noise.

(2) Intermediate Period

Two situations arise in the next phase of the mission. First, the spacecraft may circle around Jupiter and receive signals from Earth. This situation is not different from that described above, as long as occultation with respect to Earth does not occur. Then, a secondary probe, launched earlier, may have approached or penetrated the cloud layer such that spacecraft-probe communication signals pass close to the cloud layer. Our studies indicate that both refractive defocussing and absorption can each reduce the signal by 20 dB or more at S- and X-band. In the case of occultation these effects are additive. We estimate that over 100 dB signal losses may occur when rays are tangential to the cloud layer within several tens of kilometers. More detailed estimates will be considered in the future when we apply the recently completed analysis of the laboratory simulation.

(3) Occultation of a Spacecraft

The latest "interesting" stage of a mission is that in which occultation of the spacecraft by Jupiter (with respect to Earth) occurs. The spacecraft orbits at several radii distance from Jupiter's center around the planet and disappears behind it. Before it disappears it is conceivable that most Jovian noise sources now lie within the main lobe of a directional antenna aimed toward Earth (particularly if the probe is more than three or four radii beyond Jupiter). Jovian noise may then exceed set noise and the considerations of Section III.D.2 on page 30 hold because $P_e/P_N \sim S_e/S_N$. We have seen that $S_e/S_N \sim 100/\Delta\nu$ at S-band in this case. The influence of Jovian noise is reduced in this configuration by utilizing an isotropic antenna.

As the spacecraft approaches the location at which the line of sight to Earth grazes Jupiter's cloud layer, absorptive and defocussing losses increase. Because at least 20 dB of attenuation is expected, even when the line of sight is tangential at some altitude near the cloud layer, and because such a loss is presumably not tolerable, it appears that an occultation experiment will yield information only on the sparser atmosphere above the cloud layer.

V. VENUSIAN ATMOSPHERE:

Reappraisal of Venera-4,5,6 and Mariner-5 Measurements of Irregular Signal Fading

A. INTRODUCTION

Kolosov, et al. (ref. 31) published a preliminary analysis of irregular signal-strength fluctuations observed by the USSR probe, Venera-4, during its parachute descent into the densest portion of the Venusian atmosphere in October 1967. We revised this analysis in the Phase-I final report (ref. 25) to conform with more appropriate turbulence-theory statistics and with our extension of Tatarski's (ref. 32) weak-scattering theory for EM signals propagating in turbulent air. We summarize the results.

A monochromatic signal, with spatial electric field $E_o(s) = A_o(s)\exp[i\phi_o(s)]$ at points s of a line-of-sight trajectory in free space, has an electric field $E(s) = A(s)\exp[i\phi(s)]$ in the presence of turbulent air along the same trajectory. In free space, the energy flux $I_o \propto A_o^2$ will exhibit only the inverse-distance-squared dependence on pathlength L. In turbulent air, the signal with electric field E(s) becomes a constant-plus-Rayleigh-distributed phasor, i.e.

$$E(L) = E_o(L)\,[\exp(-\sigma_\varepsilon^2) + \delta B] \qquad (40)$$

In this formula, σ_ε^2 is a function of frequency, pathlength, and certain time averages of quantities describing the effect of turbulence upon electric signal. The quantity δB is Rayleigh distributed, with zero mean and $\langle|\delta B|^2\rangle = 1-\exp(-2\sigma_\varepsilon^2)$. In other words, if we know σ_ε, we then know the statistics of the amplitude A(L) or, equivalently, of the energy flux $I(L) \propto A^2(L)$.

Figure A-2 of ref. 25 presents plots of σ_ε^2 at given frequencies and altitudes (according to the Venera-4 scale corrected by 25 km) for a vertical path terminating at the probe location. From these values of σ_ε^2, we have formed the Norton parameter $K = 10\log[\exp(2\sigma_\varepsilon^2)-1]$, i.e. the ratio of powers in the two terms of Eq. (40), and thus formed conventional 99% fading-estimate plots in Fig. 1 of ref. 25.

Since the publication date of the Phase-I final report, two Russian analyses have been published. Gurvich (ref. 33) has utilized Venera-4 and Mariner-5 measurements to compute σ_ε^2 in essence. He finds an

appreciable difference between the σ_ε^2 estimated from Mariner-5 occultation measurements and the equivalent σ_ε^2 inferred from Venera-4 measurements. This difference conflicts with our preliminary Mariner-5 estimate and it must be explained. Kolosov, et al. (ref. 34), in a second publication, present Venera-5 and Venera-6 data alongside with Venera-4 data. They also analyze Mariner-5 data and find results not very different from Gurvich.

In the following two subsections, we will revise our fading estimates, based on Venera-4 measurements, to include the new Venera-5 and 6 data, and we will present a reappraisal of Mariner-5 signal irregularities based on a more careful analysis of the data.

B. REVISED VENERA-4 AND NEW VENERA-5,6 SIGNAL FADING ESTIMATES

The fading estimates of Fig. 1 of ref. 25 are obtained from the σ_ε graphs of Fig. A-2 in the same report. The σ_ε graphs for 2, 5, and 10 GHz were obtained from frequency scaling of the curve $\sigma_\varepsilon(z) = \sigma_\varepsilon(0)\exp(-z/h)$ for the 940 MHz data of Venera-4. Actually, we fitted this exponential to the value $\sigma_\varepsilon(25) \sim 0.18$ and we chose $h \approx 13$ km. Upon rechecking the calculation we find that the values of $\sigma_\varepsilon(z)$ plotted in Fig. A-2 (ref. 25) are about one half of what they should be according to the above procedure. Moreover, Yakovlev and Yakovleva (ref. 35) have reanalyzed the pressure and temperature profiles of the lower Venusian atmosphere and they obtain for $z \leqslant 30$ km (old Venera-4 altitude scale) that the refractivity $N(z) = N_o e^{-z/h}$ with $h \approx 10.4$ km (N is defined as the deviation n-1 from unity of the refractive index). For these two reasons alone it would be worthwhile to revise our estimates. Now that Venera-5 and 6 data have become available, we need no longer postpone revision.

Kolosov, et al. (ref. 34) have now made these new data available in a preliminary form. They present values of the parameter $\eta(z)$ (the ratio of standard deviation to mean signal amplitude) at various altitudes z for Venera-4,5,6. All of these values of $\eta(z)$ computed from 940 MHz data lie below $\eta = 0.1$, hence we may utilize the linear weak-scattering theory (Born approximation) and set $\eta = \sigma_\varepsilon$ as we have explained in ref. 25, Eq. A-3. We reproduce these data corrected for earth-atmospheric fluctuations in Fig. 17: Venera 4,5,6 data are denoted by circles, triangles, and squares respectively. The altitude scale is defined by the pressure scale such that z = 0 km corresponds to p = 92 atm. To put matters in perspective, we note that the altitude scales of Fig. A-2 and Fig. 1 of ref. 25 were chosen so that z = 25 km corresponds to p = 20 atm. Thus, the Venera-4 value $\sigma_\varepsilon \sim 0.18$ corresponding to the hypothesized zero altitude on the Venera-4 scale appears at $z \approx 22$ km on Fig. 17. The dashed line through it corresponds to an exponential with scale height $h \approx 13.4$ km.

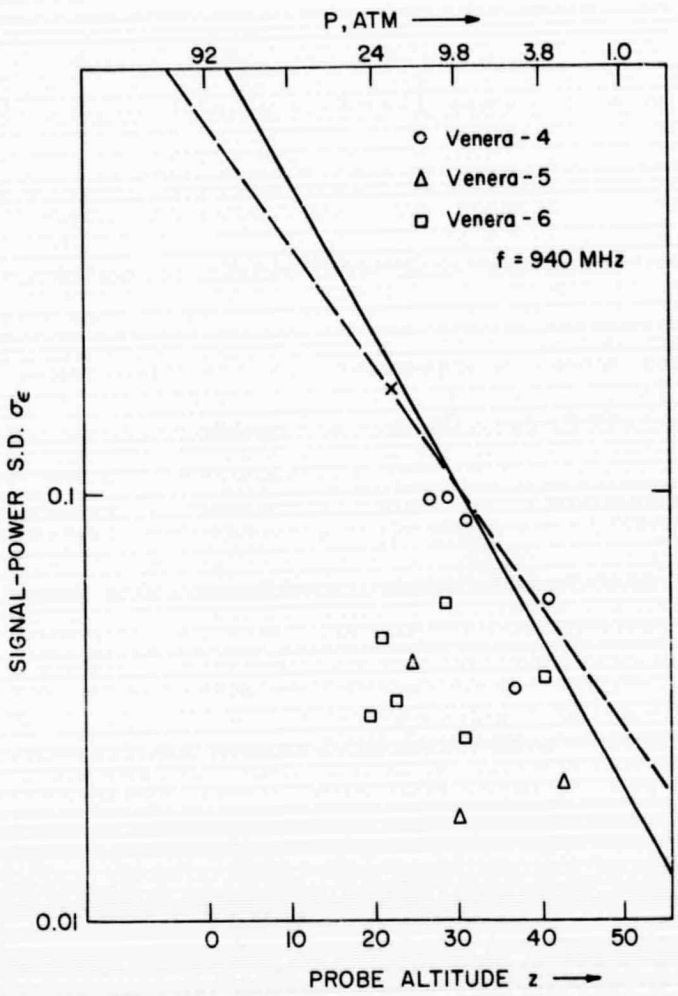

Figure 17. Normalized signal-amplitude s.d. at diverse altitudes above the 92 atm altitude in the Venusian atmosphere: Venera- 4,5,6 data.

It will be noted that the Venera-5 and-6 data points lie appreciably below the Venera-4 data; also that there is appreciable data spread. No unique procedure can be given for a σ_ϵ vs. z curve at 940 MHz in the absence of better data. The following considerations are proposed as an aid. The parameter σ_ϵ is proportional to the standard deviation of refractive index $n(z) = 1 + N(z)$. Thus, $\delta n(z) = \delta N(z)$. In the lower Venusian atmosphere ($z \lesssim 52$ km in the altitude scale of Fig. 17) we have $N(z) \approx 0.145\ p(z)/T(z)$ with p in atm and T in degrees Kelvin. It follows that $\delta N(z) = N(z)[\delta p/p - \delta T/T] \approx N(z)\ \delta\rho/\rho$ where $\rho(z)$

is the atmospheric density at altitude z. It thus follows that the root-mean-square $\delta N(z)$ scales with altitude z as the product of N(z) and the density ratio $(\delta\rho/\rho)_{rms}$. It is not clear how the ratio $\delta\rho/\rho$ scales with z. In the simplest picture of turbulence in an exponential-density atmosphere, one pictures a shearing effect due to the winds that displaces a parcel of unit mass and density $\rho(z)$ to a new altitude $z + \ell$ where it mixes with air at density $\rho(z+\ell)$. At $z + \ell$ there is a fluctuation $\delta\rho = \rho(z+\ell)-\rho(z) \sim \ell d\rho/dz$. In an exponential-density profile, $\rho^{-1}d\rho/dz = h^{-1}$ is a constant and therefore $\delta\rho/\rho \sim \ell/h$. Now, it is experienced on Earth that the distribution of scales ℓ, i.e. the magnitudes of inner- and outer-scales ℓ_o and L_o and the shape of the turbulence energy spectrum vary little over certain altitude bands. The simplest assumption, which ignores gaps in the altitude distribution of turbulence mechanisms, is therefore that $\delta\rho/\rho$ is fairly invariant with altitude. In that case we reason that δN, and thus σ_ε, scales with the refractivity N(z), i.e. $\sigma_\varepsilon(z) = \sigma_\varepsilon(0)\exp(-z/h)$. On the other hand, little is really known about Venusian atmospheric turbulence. Furthermore, objections can be raised to scaling σ_ε with the refractivity, and the Russian workers do not do so. As a "worst case" estimate, we have done the following: we have fitted a least-squares exponential to the Venera-4 data points. The result is,

$$\sigma_\varepsilon(z) = 1.175 \exp(-0.0785z) \qquad (41)$$

Note that the scale height thus defined (k = 12.7 km) is somewhat larger than that of Yakovlev and Yakovleva (ref. 35), namely $h \approx 10.4$ km, and somewhat smaller than the Martin Marietta "MMC-L" (ref. 38) model-atmosphere scale height for N (h = 15.9 km). Since most of the Venera-5 and-6 data points lie within a factor three below the exponential $\sigma_\varepsilon(z)$ of Eq. (41), we consider values of $\sigma_\varepsilon(z)$ to be uncertain by that amount.

Figure 18 gives the exponential-law $\sigma_\varepsilon(z)$ of Eq. (41) in terms of the estimated fading level in dB (i.e. the magnitude of fades below the median signal power at least 1% of the time) as described in ref. (25). The solid 940 MHz line represents Eq. (41), and the dashed one indicates the lower bound of the uncertainty due to the weaker fluctuations measured by Veneras-5 and-6. Because the solid curve corresponds to actually measured (Venera-4) fluctuations, it should probably be regarded as the worst-case estimate (aside from uncertainties about extrapolating it as we have below 25 km altitude). By scaling $\sigma_\varepsilon(z)$ with frequency first as f (upper curves), then as $f^{7/12}$ (lower curves) we obtain the 2 GHz and 5 GHz pair of curves. There is an uncertainty of that extent in the frequency scaling. To explain it, we note that

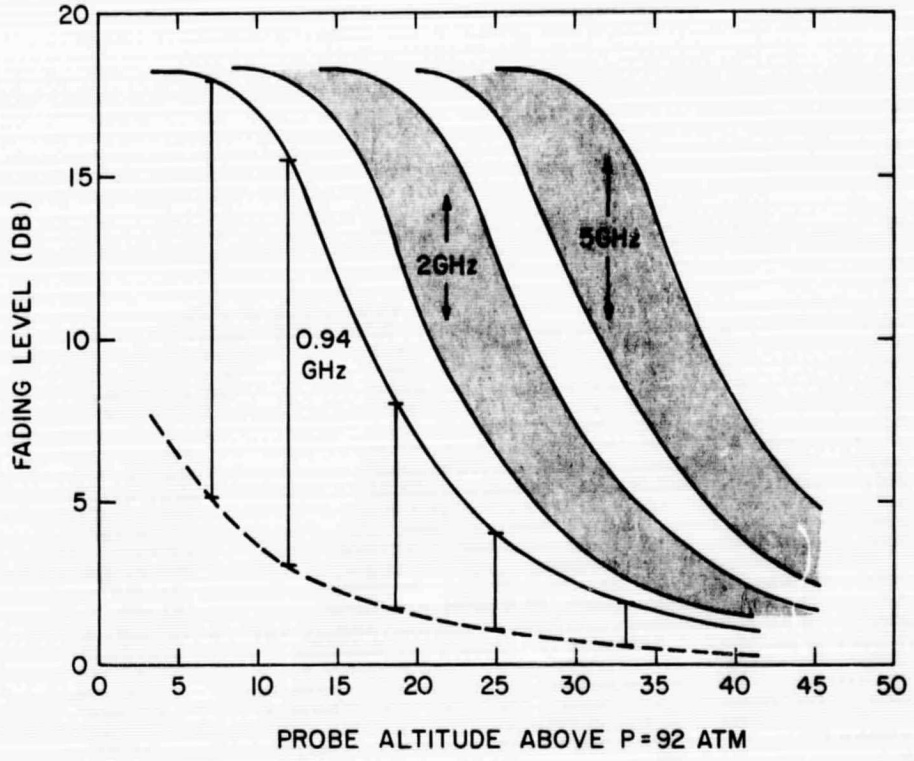

Figure 18. Estimated fading (in dB) at the 99% level (i.e. the signal strength drops below the median by at least the amount indicated on the ordinate 1% of the time) for vertical propagation through the Venusian atmosphere. Each curve is accompanied by two (dashed) error-limit curves.

$\sigma_\varepsilon^2(z)$ is given by Eq. (8a) of ref. 36 applied to an exponential atmosphere,

$$\sigma_\varepsilon^2(z) = \frac{k^2 h \varepsilon^2(z)}{32\pi\cos\theta} \int_0^\infty dKK\Phi(K)\ [1 - (1 + K^2 h/2k)^{-1}] \qquad (42)$$

Here, a line-of-sight path, at angle θ with the vertical, terminating at z is considered and $h/2\cos\theta$ is the effective pathlength. The problem in frequency scaling is determined by the fact that the factor in [ ] sets an effective lower bound $\propto (2k/h)^{1/2}$ on the dK integration. When

$(2k/h)^{1/2} \ll L_o^{-1}$, the integral of $K\Phi(K)$ hardly differs from the $K = 0$ to $K = \infty$ integral and consequently $\sigma_\varepsilon(z) \propto k$. When $(2k/h)^{1/2} \gg L_o^{-1}$ we may set $K\Phi(K) \propto K^{-8/3}$ and we obtain $\sigma_\varepsilon(z) \propto k^{7/12}$. When $(2k/h)^{1/2} \sim L_o^{-1}$ some intermediate frequency dependence ensues. At 940 MHz we find that the length $(h/2k)^{1/2} = 26.5$ m. We have indicated that the macroscale L_o may lie between 8 and 42 m depending on the assumed wind-shear velocity. Although we tend towards accepting the lower value $L_o \sim 10$ m, we cannot rule out higher values, and it may well be that $(2k/h)^{1/2} \sim L_o^{-1}$ at 940 MHz. We have therefore applied both scalings with k in Fig. 18.

Thus, Fig. 18 is presented as a revised and updated graph of signal-fading estimates due to uniformly distributed turbulence in the Venusian atmosphere, and it reflects the data spread of Venera-4,5,6 as well as the uncertainty in the macroscale L_o.

It should be noted in Fig. 18, that the portions of the solid curves below $z \approx 25$ km are extrapolations to lower altitudes of the measured Venera-4 scintillations. At 5 GHz and higher frequencies it is presumably the lower curve (corresponding to $f^{7/12}$ scaling) that is more accurate. Since a saturation level is nearly reached at 5 GHz and at 25 km altitude for this lower curve, we observe that fading at lower altitudes at 5 GHz and higher frequencies is very severe, even if $\sigma_\varepsilon(z)$ is kept constant from $z = 25$ km down to the surface. At S-band frequencies, the uncertainty is still important enough to raise a doubt about the severity of fading in the lower atmosphere.

Finally, as a footnote, we add a revised computation of $\varepsilon(z)$ because that given in Fig. (2-A) of ref. 25 is in error. Utilizing $L_o \sim 25$ m and $f = 940$ MHz (for Venera-4) we obtain, upon inverting $\sigma_\varepsilon^2 = k^2 L L_i \varepsilon^2$, a value of $\varepsilon(z) \sim 6 \times 10^{-5}$ at $z = 20$ km in agreement with Kolosov, et al. (ref. 34). The uncertainty in magnitude of L_o is reflected in this value because $\varepsilon \propto L_o^{-1/2}$.

C. REAPPRAISAL OF THE MARINER-5 SIGNAL FADING UPON OCCULTATION

Gurvich (ref. 33) and Kolosov, et al. (ref. 34) have analyzed the same Mariner-5 data we have (see Fig. 3 of ref. 25) and they find a value for σ_ε^2 which is much lower than the adjusted Venera-4 prediction for the Mariner-5 geometry. In our first reappraisal we appeared to obtain reasonable agreement with a sample calculation. The discrepancy has forced us to reexamine the data more carefully and we have come to the following conclusions:

(1) Gurvich has computed a value for σ_ε^2 that excludes fluctuations at rates less than ~ 0.1 Hz.

(2) Our sample calculation led to a σ_ε^2 that was higher because we did include slow fluctuations; we now agree with Gurvich's result after excluding the slow fluctuations.

(3) Neither Gurvich's, Kolosov's, nor our analysis can yield information on signal fading due to turbulence because the signal integration times are so long that the rapid fades due to the type of turbulence inferred from Venera-4 signal fading are smoothed out. It does not appear feasible (Kliore: private communication, Sept. 1970) to shorten the integration times appreciably because the signal-to-noise ratio is unfavorable. The Mariner-5 predictions must therefore be considered with reserve.

The above conclusions were reached after the following considerations: We have taken the data (given at 0.2 sec intervals) of Fig. 3, ref. 25, from which we wish to form $\sigma_I^2 = (\langle I^2\rangle - \langle I\rangle^2)/\langle I\rangle^2$. When $\sigma_I < 0.2$, it is a good approximation to set $\sigma_\varepsilon = \sigma_I/2$. In order to obtain an idea of the relative effect of fluctuations at different rates, we have actually computed a time-lagged quantity,

$$\sigma_I^2(\tau) = \langle [I(t) - I(t+\tau)]^2 \rangle / 2\langle I\rangle^2 \qquad (43)$$

As τ becomes larger, the autocorrelation $\langle I(t)I(t+\tau)\rangle$, computed for fixed τ, becomes $\langle I(t)\rangle\langle I(t+\tau)\rangle = \langle I\rangle^2$, and it follows that $\sigma_I^2(\tau)$ approaches the quantity σ_I^2. For fixed τ it can be seen upon Fourier analyzing I(t) with respect to t that the spectral components of I(t) with frequencies $\omega \gg \tau^{-1}$ contribute to $\sigma_I^2(\tau)$ as they would to σ_I^2, whereas components at $\omega \ll \tau^{-1}$ contribute negligibly. The effect of forming $\sigma_I^2(\tau)$ is to eliminate low-frequency contributions to σ_I^2. We have sampled the data at 0.4-sec intervals (every other point; the difference with optimal 0.2-sec intervals is unimportant) and formed $\sigma_I^2(\tau)$ for $0 < \tau \lesssim 15$ sec. The result is displayed in Fig. 19 for two time spans: 1738:20 to 1739:00 min (39.9 to 37.7 km) and 1739:30 to 1740:10 min (36.5 to 35.3 km). The altitude scales have been chosen to correspond to 0 km at 92 atm of pressure, using Fig. 2 of Eshleman et al. (ref. 37). We note that $\sigma_I^2(\tau)$ is a monotonically increasing function of τ and thus the choice of τ is cardinal. The later time span exhibits a sharp increase at $\tau \sim 8$ sec; the large dip at 1740 min is being felt at this stage. Kolosov, et al. (ref. 34) argue that this dip is not due to turbulence but to an inversion of the refractivity. We agree that the dip cannot be due to turbulence.

This brings us to the next point of importance: the data are sampled at 0.4 sec and it appears that the sampling cannot be improved

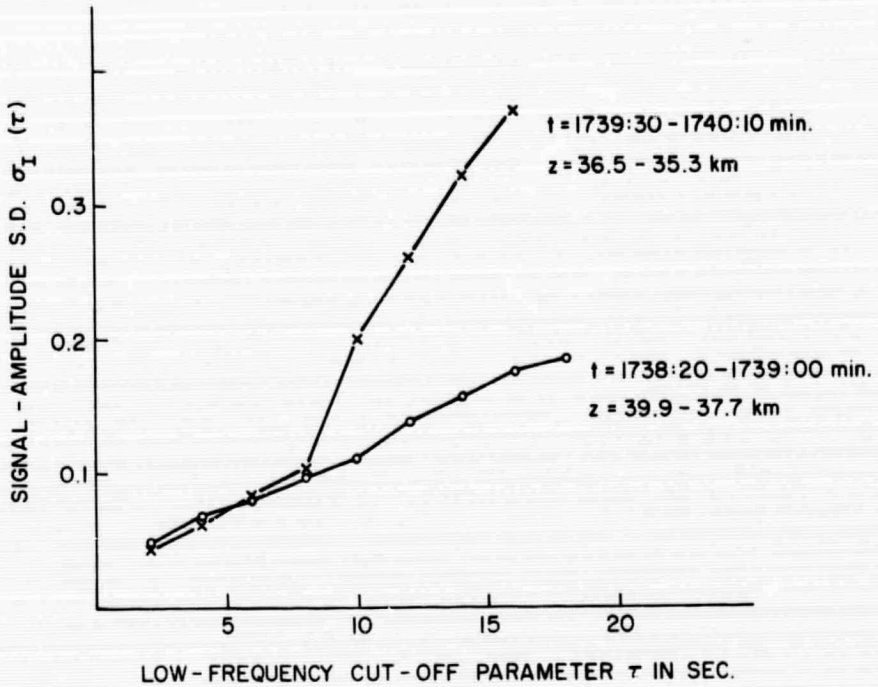

Figure 19. Normalized signal-power s.d. of Mariner-5 S-band occultation signals with low-frequency cut-off at τ^{-1} Hz for two data spans of 40 sec.

by more than a factor of two because a 0.1- to 0.2-sec integration of signal was required to overcome noise problems. This sets an upper bound of 2.5 to 5 Hz on the range of fluctuation frequencies that can be analyzed from the data. Let us now consider the mechanism giving rise to temporal fluctuations of signal strength in the case of Mariner-5. Two processes compete; the intrinsic churning motion of the eddies (at velocities of perhaps several m/sec) and the sweeping motion of the line of sight through the eddies to lower altitudes. The latter motion is at velocities of 35 and 65 m/sec for the two data spans, and these velocities are so much higher that the sweeping motion prevails. Let U be the sweep velocity. The range of spectral frequencies lies between U/ℓ_o and U/L_o, i.e. the low-frequency cut-off lies in the neighborhood of U/L_o. Estimates of L_o range from 10 to 50 m. Consequently estimates of U/L_o range from 0.7 to 3.5 Hz. We therefore expect turbulence to give rise to fluctuations at rates higher than 0.7 to 3.5 Hz. On the other hand, the Mariner-5 signal fading yields fluctuations at frequencies less than 2.5 to 5 Hz. *We conclude that only a small fraction of turbulence effects can have been observed;* most of the fading must occur at higher, unobservable rates.

In order to verify this further we note that $\sigma_I(\tau) < 0.088$ for $\tau < 5$ sec. Thus we find $\sigma_\varepsilon < 0.04$ excluding fluctuations at rates less than 0.2 Hz. In order to convert to a Venera-4 situation we must divide this value by $(4\pi R/h)^{1/4} \approx 9.3$ and by 2.4 [or $(2.4)^{7/12}$] to scale to 940 MHz. The result for a Venera-4-like fading strength at 940 MHz and at an altitude of 35 to 40 km is $\sigma_\varepsilon < 3 \times 10^{-3}$, i.e. at one to two orders of magnitude below the observed Venera-4,5,6 normalized standard deviations. As we have discussed above, this is due at least in part to the exclusion of most of the frequency range of turbulent fluctuations from observation.

Thus, we have found - as the Russian workers appear to also - that the Mariner-5 data yields much lower values of C_n^2 than Venera-4. In our opinion, this is because turbulence-induced fading is smoothed out of the Mariner-5 data upon processing. We have not attempted to compute C_n^2, or $\varepsilon^2 = \langle(\delta\varepsilon)^2\rangle$. Equation (41) can be used, but - we stress - with caution because macroscale L_o cannot be determined with any certainty. Russian workers utilize a plane-wave form of Eq. (41) and assume that $(h/2k)^{1/2} << L_o$ to obtain $\sigma_\varepsilon^2 \propto k^2 L_i L \varepsilon^2$, where L_i is the integral scale. The inversion yields ε^2, but because L_i is basically unknown we really obtain the product $L_i\varepsilon^2$. Attempts to estimate L_i and ε^2 separately have been discussed previously (ref. 25).

VI. NEW TECHNOLOGY APPENDIX

While the work performed under this contract had led to improved understanding of the communications medium, no technological innovation was made.

REFERENCES

1. J. R. Dickel, J. J. Degioanni, and G. C. Goodman, The Microwave Spectrum of Jupiter, Radio Science 5, 517 (1970).
2. D. D. Thornton and W. J. Welch, 8.35 mm Radio Emission from Jupiter, Icarus 2, 228 (1963).
3. G. C. Goodman, *Models of Jupiter's Atmosphere*, Ph.D. thesis, University of Illinois, Urbana (1969).
4. C. M. Michaux, Handbook of the Physical Properties of the Planet Jupiter, (NASA SP-3031, Douglass Aircraft Company, Inc. Santa Monica, Calif. (1967).
5. V. I. Moroz, *Physics of Planets* (Tech Translation NASA TTF-515, Washington, D. C., 1968).
6. L. M. Trafton, Model Atmospheres of the Major Planets, Astrophys. J. 147, 765 (1967).
7. T. Owen, The Atmosphere of Jupiter, Science, 167, 1675 (1970).
8. C. M. Michaux, op. cit., pp. 99.
9. C. H. Townes and A. L. Schawlow, *Microwave Spectroscopy* (McGraw-Hill, New York, 1955).
10. A. Ben-Reuven, Impact Broadening of Microwave Spectra, Phys. Rev. 145, 7 (1966) and Phys. Rev. Letters 14, 349 (1965).
11. B. Bleaney and J. H. N. Loubser, The Inversion Spectra of NH_3, CH_3Cl, and CH_3Br at High Pressures, Proc. Phys. Soc. 63A, 483 (1950).
12. A. A. Maryott, (Private communication).
13. G. T. Wrixon, Microwave Absorption in the Jovian Atmosphere (Univ. of Calif. Lab. Rep., Ser. 10, issue 26, 1969).
14. B. A. Sodek Jr., J. Spacecraft and Rockets 5, 461 (1968).
15. Handbook of Chemistry and Physics (Chemical Rubber, Cleveland, 1961).
16. D. E. Kerr ed. *Propagation of Short Radio Waves* (McGraw-Hill, New York, 1951).
17. A. Kliore, et. al., Science 158, 1683 (1967).
18. G. Birnbaum, S. J. Kryder, and H. Lyons, J. Appl. Phys. 22, 95 (1951).
19. J. D. Jackson, *Classical Electrodynamics* (Wiley, New York, 1962, p. 256).
20. G. Birnbaum and A. A. Maryott, Phys. Rev. 92, 270 (1953).

21. G. Birnbaum and A. A. Maryott, Jour. Chem. Phys. 21, 1774 (1953).

22. E. C. Morris and R. W. Parsons, Aust. Jour. Phys. 23, 335 (1970).

23. J. S. Lewis, Icarus 10, 365 (1969); Icarus 10, 393 (1969).

24. W. Ho, I. A. Kaufman, and P. Thaddeus, Jour. Geophys. Res. 71, 5091 (1966).

25. D. A. de Wolf and J. W. Davenport, Investigation of Line-of-Sight Propagation in Dense Atmosphere: Phase I, NASA CR-73440 (March 1969 - May 1970).

26. J. A. Stratton, *Electromagnetic Theory* (McGraw-Hill, New York, 1941).

27. C. M. Michaux, op. cit., Fig. 8.1.

28. G. R. Blumenthal and R. J. Gould, Rev. Mod. Phys. 42, 237 (1970), Section 4.4.

29. D. B. Chang and L. Davis Jr., Astrophys. J. 136, 567 (1962).

30. J. N. Clark, Radio Sci. 5, 529 (1970), p. 533.

31. M. A. Kolosov, O. I. Yakovlev, and A. I. Yefimov, Study of the Propagation of Decimeter Radiowaves in the Atmosphere of Venus with the Aid of AIS "Venera-4", Doklady, A. N. SSSR, Geofizika 182, 93 (1968), translation available from CFSTI, Springfield, Va. 22141, under accession number NASA CR 97015.

32. V. I. Tatarski, *Wave Propagation in a Turbulent Medium*, Translation R. A. Silverman (McGraw-Hill, New York, 1961).

33. A. S. Gurvich, An Estimate of the Small-scale Turbulence Parameters in the Venus Atmosphere by Radio Signal Fluctuations of "Venera-4" and Mariner-5", (in Russian) Doklady, Akad. Nauk. SSSR, Fizika Atmosfery i Okeana 5, 1172 (1969).

34. M. A. Kolosov, O. I. Yakovlev, G. D. Yakovleva, and A. I. Yefimov, Radio Wave Fluctuations and Refraction Coefficient Variations in the Venusian Atmosphere, COSPAR Meeting (paper m 23) Leningrad, May 22, 1970.

35. O. I. Yakovlev and G. D. Yakovleva, Propagation of Ultrashort Waves in the Atmosphere of Venus, Radio Eng. & Electr. Phys. 14, 503 (1969).

36. D. A. de Wolf, Spherical Waves Through a Random Continuum, Radio Sci. 2, 1513 (1967).

37. V. R. Eshleman, G. Fjeldbo, J. D. Anderson, A. Kliore, and R. B. Dyce, Venus: Lower Atmosphere Not Measured, Science 162, 661 (1968).

38. Martin Marietta Corp., 1975 Venus Multiprobe Mission Study, Final Report on JPL Contract 952534, April, 1970.